Universiteit Utrecht

Objective detection and quantitative analyses of a Shoreward Propagating Accretionary Wave in a double sandbar system

MSc Thesis

Version 2

06-02-2017

Liza de Wit 5608260

Supervisors

Dr. T.D. Price

Prof. Dr. B.G. Ruessink

Faculty Geosciences

Department of Physical Geography

Title

Objective detection and quantitative analyses of a Shoreward Propagating Accretionary Wave in a double sandbar system

Pages

72

Keywords

Bar dynamics, SPAW, Beach Wizard, assimilation, nearshore processes, Argus

Summary

A shoreward propagating accretionary wave, or SPAW, is a bar like feature that is shed off from the landward side of a bar and subsequently migrates through the trough and eventually merges with the beach or the more shoreward (inner) sandbar. A SPAW event between 09-07-2001 and 07-09-2001 near the beach of Egmond aan Zee, The Netherlands, was studied. During the event the SPAW migrated from the outer towards the inner sandbar. On the basis of time-exposure images and wave data, the roller dissipation maps were computed and used together with an initial bathymetric map in an assimilation model to estimate the bathymetry during the study period. To include the SPAW in the assimilation process, existing methods developed by Aarninkhof and Ruessink (2004) were adapted. Previous studies only included the intensity peaks over the sandbars; the adaption involved the intensity peak between the inner and the outer sandbar, caused by the SPAW, to be included in the calculation of the roller dissipation maps. The estimated bathymetric maps show the presence of the SPAW between the inner and the outer sandbar. The average SPAW width, length, height and volume are 70 m, 290 m and 0.7 m, respectively. The width and length found by the assimilation model are higher than the width and length found in time-exposure images, which are 31 m and 218 m, respectively. Not the whole lifecycle of the SPAW was captured: once the SPAW could be detected in the bathymetric maps it was already closer to the inner sandbar than to the outer bar. During the time the SPAW could be detected in the bathymetric maps the SPAW width and length increased, this is in contrast with previous research on SPAWs that stated that the SPAW maintained its shape. A comparison between the SPAW event in the bathymetric maps and event in the time-exposure images showed the SPAW dimensions and dynamics for the two sources did not correspond directly.

Contents

1. Introduction

Sandy wave-dominated beaches characterize the Dutch coast. These beaches often show one or more sandbars within the first 100 meters of the shoreline. Sandbars are submerged ridges of sand and in a way a natural barrier between the hinterland and the ocean and thus protect the beach and the dunes from erosion by wave action (Koster, 2006; Van der Weerd, 2012, Price et al., 2014). Besides protection against flooding, the coast also provides other ecosystem services, such as recreation, commerce and biodiversity (Holman & Haller, 2013), making them of valuable significance. Despite this, much is still unknown about nearshore and shallow water processes influencing the morphodynamics of sandy coasts. During storms sand erodes from the dunes and is transported seaward, however during calm weather conditions sand is transported landwards. The mechanisms driving this landward transport are poorly understood.

To protect the Dutch coast from erosion, each year a volume of 12 Mm^3 sand is being deposited in the surfzone through shoreface nourishments. This deposited sediment is indented to migrate landward and feed the beach-dune system (Baptist et al, 2009). As such, mechanisms driving landward sediment transport are of great importance for the planning of shore face nourishments.

Wijnberg and Holman (2007) studied a phenomenon that might help shed light on these mechanisms. They called this phenomenon a Shoreward Propagating Accretionary Wave, or SPAW. This is a bar like feature that is shed from the landward side of a sandbar and subsequently migrates through the trough and finally merges with the beach or the more shoreward (inner) sandbar (Wijnberg and Holman, 2007; Van der Weerd, 2012; Almar et al., 2010). A SPAW can be seen as a small-scale natural mode of shoreface nourishment (Van der Weerd, 2012).

Previous research has shown that SPAWs represent a steady onshore directed sediment flux (Wijnberg and Holman, 2007; Van der Weerd, 2012; Almar et al., 2010).

This study aims to improve the understanding of SPAWs, more insight into this topic aids in a better understanding of coastal dynamics.

2. Literature Research

In this chapter the current state of knowledge about the nearshore environment, sandbars and SPAWs is summarized. The chapter concludes by identifying the research gap and formulating the research questions as the starting point for further analysis.

2.1. Nearshore environment

The nearshore zone is a small part of the ocean that borders continents and consists of (i) the shoaling zone, where the water depth decreases, (ii) the surfzone in which the waves break and (iii) the swash zone, this is the region where the waves run up to the beach (Holman and Haller, 2013; Masselink et al., 2003). As sandbars are located in the nearshore zone, in this paragraph processes and mechanisms relevant for SPAW dynamics will be discussed in the following order; waves (section 2.1.1), currents (section 2.1.2) and sediment transport (section 2.1.3).

2.1.1. Waves

Waves are generated by wind moving across the surface of the water. The friction between the air molecules and the water molecules causes energy to be transferred from the wind to the water, causing waves (Masselink et al., 2003).

2.1.1.1. Wave energy

The propagation of a wave comprises a transfer of energy over the sea surface. Waves derive their energy from two sources: potential and kinetic energy. Potential energy is associated with the deformation of the water surface from a reference level. Kinetic energy is generated due to the orbital motion of water particles. The total amount of energy consists of the sum of potential and kinetic energy. The equation for the total amount of energy (E) per unit area [N/m2):

$$E = \frac{1}{8}\rho g H^2{}_{rms} \quad (1)$$

Where ρ is the density of the water [kg/m3], g is the gravitational acceleration (m/s^2) and is H_{rms} the root mean square wave height [m]. As can be deducted from the above equation is the total amount of energy directly related to wave height. Wave energy depends on the square of the wave height; consequently a doubling in wave height would result in a fourfold

increase in wave energy. The rate at which wave energy is carried along by the moving waves can be defined as the wave energy flux (P).

$$P = E\ C\ n = \ E\ \mathrm{Cg} \tag{2}$$

Where C is the wave is phase velocity [m/s] and Cg is the wave group velocity (m/s). The parameter n increases from 0.5 to 1 from deep to shallow water; deep water waves travel twice the speed of the wave groups (n =0.5), in shallow water however waves propagate at the same speed as the wave groups (n =1). Wave groups are formed by the merging of two wave trains, of different wave lengths but the same amplitude (Masselink et al., 2003; Holthuijsen, 2007).

2.1.1.2. Wave Processes

Shoaling

The shoaling zone is located just landward of the deep water zone. In this zone the waterdepth decreases and the wave height increases, the latter is called shoaling. As the waves approach the shore and enter shallower water the depth decreases and thus the wave velocity decreases.

$$C = \sqrt{g * h} \tag{3}$$

The energy flux however should remain constant; to compensate for the decrease in wave velocity the wave energy should increase. For the wave energy to increase the wave height must increase, hence shoaling (Masselink et al., 2003).

Wave breaking

At some point the water depth becomes too shallow for a stable waveform to exist and waves break. The instability occurs when the horizontal velocities of the water particles in the wave crest exceed the velocity of the wave form: the particles leave the wave form, which disintegrates with bubbles and white foam (Masselink et al., 2003).

Skewness and asymmetry

In deep water waves have a perfect symmetric sinusoidal shape and water particle velocities associated with the wave motion are symmetrical: onshore velocities are as strong as offshore velocities. However, when waves enter shallower water waves deform. Deformation can take place in the sense of skewness, asymmetry or both (Masselink, 2003; Holthuijsen, 2007).

Skewness

Waves are deformed into skewed waves in the shoaling zone, where the wave crest is peaky and the wave trough is more flat. This results in a short period of relative high positive flow velocities under the crest and a long period of relative low flow velocities under the trough (Holthuijsen, 2007). Skewed waves induce the onshore transport of sediment: the short duration high onshore flow velocities transports more sediment in the onshore direction than the long duration low offshore flow velocities in the offshore direction.

Asymmetry

As waves propagate further towards the breaking zone the waves' skewness decreases, but now the waves become asymmetric. Asymmetric waves show a steep rise from peak ebb velocities to peak flood velocities, and a slow fall from peak flood velocities to peak ebb velocities (Holthuijsen, 2007). Asymmetric waves also cause onshore sediment transport of sediment, this onshore transport can be linked to the different time spans in which the positive (onshore) and negative (offshore) flows are dominant.

2.1.2. Currents

Currents are driven by gradients like wave energy and wave set up. In this section current driven by both tides and waves are discussed.

2.1.2.1. Tide driven currents

Tides are periodic movements of which amplitude and phase can be related to geophysical forcing. The most important geophysical forcing function is the variation of the gravitational field on the surface of the earth, caused by the regular movements of the moon-earth and earth-sun systems (Pugh, 1996). The regular movement of water is seen as long waves that cause a difference between low and high water (tidal range). A distinction is made between the vertical and horizontal tides. The vertical tide refers to the water elevation and the horizontal tide refers to the tidal flow velocity (Bolle et al., 2010). Especially the vertical tide

can be of great importance due to the difference in sediment transport during high tide and low tide. During low tide a wave might break on the SPAW while during high tide the wave will not break over the SPAW. In the Netherlands alongshore coastal currents caused by the tides are northward directed during flood and southward directed during ebb.

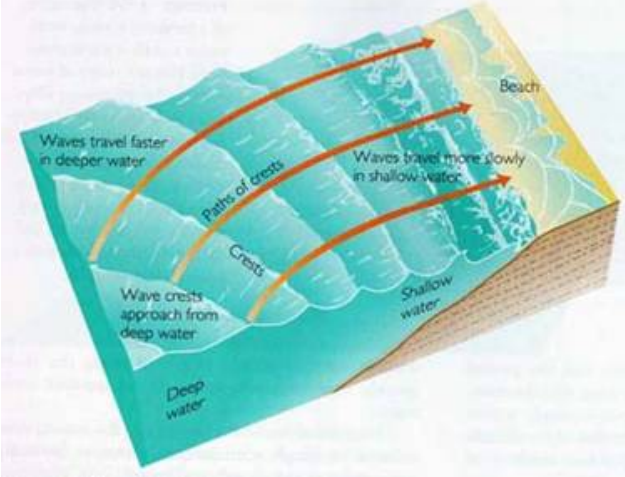

Figure 1 Schematic overview of the process of refraction where an obliquely incident wave approaches the coast with a changing direction (citation needed)

2.1.2.2. Wave driven currents

Nearshore circulation

Nearshore circulation is dominated by wave-induced forces associated with shallow water wave breaking. This type of circulation is confined to a small area near the shore (Battjes et al., 1990). A SPAW in a sense is a small sandbar, and thus a more comprehensive understanding of circulation patterns around sandbars can help understand the mechanisms driving the SPAW migration. Waves transport not only energy but also momentum. This momentum transport acts as a horizontal stress in the water, so-called radiation stress. Due to the increase in overall energy in the shoaling zone compared to the deep water zone a positive gradient in radiation stress is generated in the direction of wave propagation. To compensate for this gradient the water level is locally lowered in the shoaling zone (Longuet-Higgins and Stewart, 1964; Holthuijsen, 2007; Masselink et al., 2003). In the surfzone where waves break energy is being dissipated. Compared to the shoaling zone the total amount of energy is lower. As a result a negative gradient in radiation stress is generated in the direction of wave propagation. In the surfzone zone the water level is increased to

compensate for this gradient in radiation stress (Longuet-Higgins and Stewart, 1964; Holthuijsen, 2007; Masselink et al., 2003). Alongshore variations in wave setdown and wave setup caused by alongshore morphological variability can cause a gradient in waterlevel (Masselink et al., 2003; Holthuijsen, 2007). A gradient in waterlevel can drive currents and result in a circulation pattern. In section 3.2 circulation patterns in double barred sandbar systems are discussed.

Alongshore currents

Alongshore currents driven by wave action are caused by refraction. Refraction is a process in which an obliquely incident wave approaches the coast and slowly changes in direction when entering more shallow water. As the wave propagates towards the coast with an angle the waterdepth will vary along the wave crest. If the wave is in intermediate or shallow water, the velocity will also vary along the wave crest with the deeper water part of the wave propagating at a faster rate than the shallower water part of the wave. The process of one part of the wave traveling faster than another part of the wave causes the angle of incidence to decrease (schematic overview in Figure 1) (Masselink et al., 2003).

Undertow

Undertow is generated when waves break. Breaking waves transport mass towards the coast between the wave crest and the wave trough. A beach is a closed system; water would pile up if there would not be a compensating return flow in the seaward direction. The compensating return current is referred to as undertow. The strength of the undertow current depends on the strength with which the waves break, which in turn is determined by wave conditions and bathymetry (Masselink et al., 2003; Van der Weerd, 2012).

2.1.3. Sediment transport

Sediment transport defined by Van Rijn (2007) as the collective movement of particles along a natural bed of the same sediment material is not well understood yet. A SPAW is a subtidal feature that migrates due to sediment transport. More knowledge of the active sediment transport processes in the surfzone can therefore contribute to a better understanding of SPAW dynamics as well.

Besides hydrodynamics the movement of sediment particles is determined by the characteristics of the material like grainsize, density, fall velocity and shape. Two types of transport can be distinguished: suspended load transport and bed load transport. Suspended sediment load transport is defined as that part of the transport where the weight of the particles can be supported by fluid turbulence. Bed load transport is the transport of particles by rolling, sliding and saltating. Initiation of motion of bed load in steady flow is defined to occur when the dimensionless bed-shear stress is larger than the threshold value. This threshold value depends on the hydraulic conditions near the bed, the particle shape and the particle position relative to the other particles (Van Rijn, 2007 (a); Van Rijn, 2007; Masselink *et al.*, 2003).

Both wave action and currents are able to transport sediment in cross- and longshore direction. In the cross-shore direction a net direction of sediment transport can cause for example the migration of features like SPAWs.

Current driven sediment transport

Currents can also cause a net sediment transport for example when the velocity pattern of currents changes due to decreased waterdepth. Another example of net sediment transport is undertow. This wave driven current transports sediment offshore, especially during storms this offshore transport can be significant. During high wave events much sediment is being entrained mainly in the lower part of the water column where undertow is present.

If the undertow is the dominant transport mechanisms this can cause severe erosion (Van der Weerd, 2012).

Wave driven sediment transport

Waves may cause a net sediment transport especially during high wave events when a lot of sediment can become entrained and be brought up into the water column. Net transport however will only occur when the shape of the wave is no longer sinusoidal, but deformed (Van Rijn, 2007; Masselink et al., 2003). Particles have a lot of time to settle during the in strength decreasing onshore flow. So before the negative flow direction sets in all the particles that were stirred and moved have had a lot of time to settle. The time span of the negative flow however is very short: the sediment has had no time to settle. When the positive flow sets in sediment both in suspension and from the bed is transported towards

the shore. Asymmetric waves can only transport suspended sediment. Bed load sediment can only be transported when the peak flow velocities during negative and positive flow are different (Van Rijn, 2007 (a); Van Rijn, 2007; Masselink *et al.*, 2003).

2.2. Sandbars

In this section the current knowledge about single and double sandbars will be analyzed. This also includes the system according to which they are classified as well as the mechanisms which are known to be held responsible for sandbar dynamics.

2.2.1. Single barred systems

Sandbar dynamics are discussed in terms of alongshore and cross-shore behavior.

Alongshore behavior

Sandbars show many variations in spatial and temporal states: from alongshore uniform (linear) to alongshore variable with a sequence of horns and bays (crescentic). For the classification of single sandbars the most widely accepted system is the one developed by Wright and Short (1984) (Price and Ruessink, 2011; Price et al., 2014) (Figure 2). This study identifies two endmembers: the dissipative and the reflective state, which are related to high and low energetic conditions, respectively. In between the endmembers several intermediate states can be identified; longshore bar and trough (LBT), rhythmic bar and trough (RBT), transverse bar and rip (TBR) and low tide terrace (LTT) (Wright and Short, 1984). During low energy conditions the downstate sequence allows the development of alongshore variability in the sandbars towards the reflective state. The timespan of such a sequence generally is one to two weeks (Van Enckevort et al., 2004). With high energy conditions an upstate sequence occurs, however not as gradual as the downstate sequence: during severe weather events all alongshore variability can be erased within hours (Van Enckevort and Ruessink, 2002(a)). High waves with an oblique angle of incidence induce the strength of alongshore currents. These relatively strong currents can straighten out the outer bar (Ruessink, et al., 2007; Price and Ruessink, 2011; Masselink et al., 2003).

Cross-shore behavior

Besides straightening of the outer bar it has been observed that during high energy weather events an offshore migration of sandbars can occur, this in contrast with the onshore migration of sandbars associated with low energy weather events (Lageweg et al., 2013;

Castelle et al., 2010 (a); Price and Ruessink 2011; Van Enckevoort, 2004). The exact mechanisms driving the on- and off- shore migration of the bars are still poorly understood. The offshore migration of sandbars during high wave events is being linked to the increased strength of wave breaking resulting in a strong undertow which leads to offshore directed sediment transport Ingle, 1966; Greenwood and Davidson-Arnott, 1979; Gallager et al., 1998). The onshore migration during mild weather is associated with wave non-linearity. Both processes of sediment transport have been discussed in section 2.3.

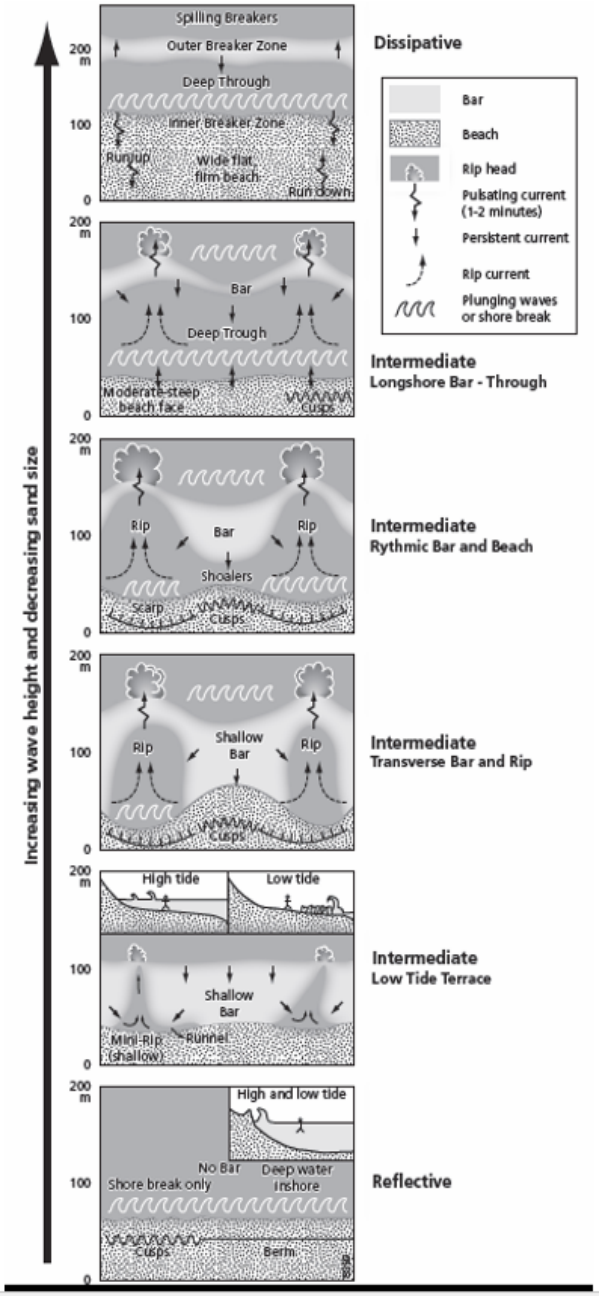

Figure 2 Schematic overview of the beach classification for single sandbars developed by Wright and Short (1984).

2.2.2. Double barred systems

Short and Agaard (1993) created a model showing that both the bars in a double barred system can go through the same intermediate states as the single sandbars as defined by Short and Wright (1984) (Figure 2). Various observations have shown that the outer bar evolves more slowly and remains in a more dissipative state than the inner bar (Ruessink, et al., 2007; Price and Ruessink, 2011; Van Enckevoort et al., 2004). Price and Ruessink (2011) adapted the Wright and Short (1984) classification scheme for double sandbar systems, where two bar states were added relative to the inner and outer bar. Observations from the northern Gold Coast, Australia show that both inner and outer bar were found to attain the erosive transverse bar and rip (eTBR) state, characterised by the alongshore uniform barline and discontinuous trough with obliquely orientated rip channels, related to the dominant oblique angle of wave incidence of the study site. Furthermore, the inner bar was dominantly observed as a rhythmic low tide terrace (rLTT), characterised by a quasi-rhythmic barline and a discontinuous trough.

An important element in the description of the intermediate states in both the classification for single and double barred system, is the the degree to which the shoreline pattern reflects the sandbar patterning (Wright and Short, 1984), and the degree of attachment of the inner bar with the shoreline (Price and Ruessink 2011). Van Enckevort et al. (2014) found, based on observations in both single barred beaches and doubled-barred beaches that systems with larger volumes of sand would respond slower to changes in energy conditions than systems with smaller volume.

2.2.3. Crescentic sandbars

SPAWs emerge from the horns from crescentic sandbar. As such, understanding crescentic sandbar behaviour can improve the understanding of SPAW formation. Crescentic bars are often part of an accretionary or downstate sequence where the crescentic bars developed from an alongshore uniform bar after a storm event. The development of these rhythmic patterns was first studied in 1888 by Lane. It was however not before the 1990s that scientists started to research the mechanisms behind these patterns. In recent years a paradigm shift has taken place from template forcing to self-organization mechanisms to explain the alongshore variability in sandbars (Coco and Murray, 2007).

The forcing template considers alongshore phase-coupling of standing edge waves as the forcing mechanism by imprinting the pattern of near-bed velocities on the seabed, generating crescentic patterns in the morphology (Holman and Bowen, 1982). This approach assumes that no feedback mechanisms exist between the morphology and the hydrodynamics. However, field observations have shown that the low flow velocities associated with edge waves are unlikely to cause the development of crescentic bars (Coco and Murray, 2007; Bryan and Bowen, 1997). Furthermore, Van Enckevort et al. (2004), based on observations of crescentic bars, determined that the patterns mainly develop during low energy conditions when the edge waves energy is lower, and a morphologic reset happens during storms when the edge wave energy is larger. As such, the forcing template model rejected as mechanism to explain the alongshore variability of crescentic bars.

The forcing mechanism was challenged by the self-organizing mechanism, where feedback between morphology and hydrodynamics is taken into account (Castelle et al., 2010 (a); Coco and Murray, 2007). This mechanism is based on the growth of one small perturbation in the bed caused by feedback mechanisms between morphology and hydrodynamics. Wave set up is locally induced at the locations of the perturbations, where the water depth is smaller. The cross-shore gradient in the radiation stress is compensated by a wave set-up landward of the perturbation. This wave set-up is larger than on the sides of the perturbation where water depths are larger, generating an alongshore flow away from the perturbation. When two positive perturbations are separated by a negative perturbation where the water depth is larger, the alongshore currents generated due to the wave breaking on the perturbations meet halfway and are pushed offshore over the negative perturbations. Therefore, a wave driven circulation pattern is generated with onshore flow over the growing horns and a strong offshore flow through the eroded bays; developing the alongshore variability of the crescentic bar (Van Enckvort et al., 2004; Coco and Murrey, 2007). The offshore flow is mainly characterized as a narrow jet of seawater flowing offshore designated as rip channels (Quartel, 2009).

2.2.4. Sandbar Coupling

The self-organization mechanism explains the morphological of the inner and the outer bar individually. Observations of double barred system often show identical alongshore spacing between horns and bays in both inner and outer bar (Ruessink et al., 2007; Castelle et al.,

Quartel 2009; 2010; Price and Ruessink, 2013). These identical patterns on both outer and inner bar suggest a morphological coupling between the crescentic bars.Different types of morphological coupling exist; (i) out of phase coupling and (ii) in phase coupling. In double sandbar systems the circulation pattern determines whether out of phase or in phase coupling occurs (Castelle et al 2010; Price et al., 2014; Sonu, 1973).

Out of phase coupling

A large fraction of wave breaking over the crescentic outer bar causes out of phase coupled sandbars. As waves propagate towards the outer bar they first break on the bay part of the outer bar. The set-up just at the bay part is stronger than on the left and right part of this location, this gradient in setup creates a rip to form. In addition more shoreward the waves break on the horn part of the outer bar, again a gradient in set-up is formed, creating a current (Figure 3a) (Price and Ruessink, 2011; Price and Ruessink, 2013).

In phase coupling

On the other hand there is in phase coupling. In phase coupling occurs when the waves are not energetic enough to break on the outer bar. However the bars do influence the hydrodynamics conditions; shoaling and refraction occur. As the waves move towards the horn of the outer bar they refract towards the horn causing the energy of the waves to be concentrated. As the waves propagate further towards the inner bar breaking occurs. The breaking is stronger on the location with the concentrated energy, causing a gradient in setup (Figure 3b) (Price and Ruessink, 2011).

The coupling between sandbars and shoreline is controlled mainly by three processes and physical parameters (van de Lageweg, 2013). Firstly, the previously discussed process of waterdepth variability in alongshore direction causing different types of circulation patterns resulting in out of phase or in phase coupling (Price et al., 2014; Ruessink et al., 2007; Van de Lageweg, 2013; Almar et al., 2010). Secondly, the angle of wave incidence which may cause variations in either up- or down state sequences. Accordingly, a downstate sequence, involving more alongshore variability increases the strength of coupling, in contrast with the downstate sequence as discussed in this paragraph before (Price et al., 2013; Price et al., 2014; Thiebot et al., 2012). The third parameter is the cross-shore distance between the

inner and the outer bar. The distance between the inner and the outer bar determines the degree as to which the sandbars interact (Van de Lageweg, 2013; Price and Ruessink, 2011).

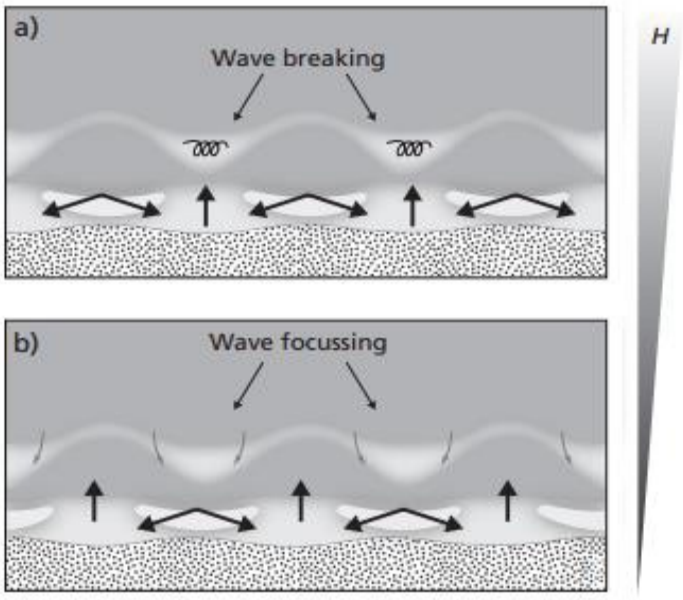

Figure 3 Coupling patterns found by Castelle *et al.* *(*2010a), showing (a) out of phase coupling and (b) in phase coupling depending on the energy conditions. Thick black arrows indicate flow patterns and grey arrows indicate refraction patterns (adopted from Price et al., 2014).

2.3. SPAWs

Wijnberg and Holman (2007) were the first to name the bar like feature that is shed from the landward side of a sandbar a SPAW, this bar like feature had been observed before by Greenwood and Davidson-Arnott (1975), Konicki and Holman (2000), Koster (2006) and Shand (2007). After Wijnberg and Holman (2007), SPAWs were studied by Almar et al. (2010), Van der Weerd (2012) and Van Kuik (2016). This section aims to describe the lifecycle of a SPAW and to compare and discuss previous research on SPAWs.

2.3.1. Definition SPAW

A SPAW is a bar like feature that is shed off from the landward side of a bar and subsequently migrates through the trough and eventually merges with the beach or the more shoreward (inner) sandbar (Figure 4) (Wijnberg and Holman, 2007). Wijnberg and

Holman (2007) found that there are similarities between a SPAW and a wave in fluid dynamics; both phenomena involve an isolated feature that moves mass in the direction of propagation, therefore calling it a wave.

The lifecycle of a SPAW can be divided in three phases; formation, migration and finally welding with the beach/sandbar.

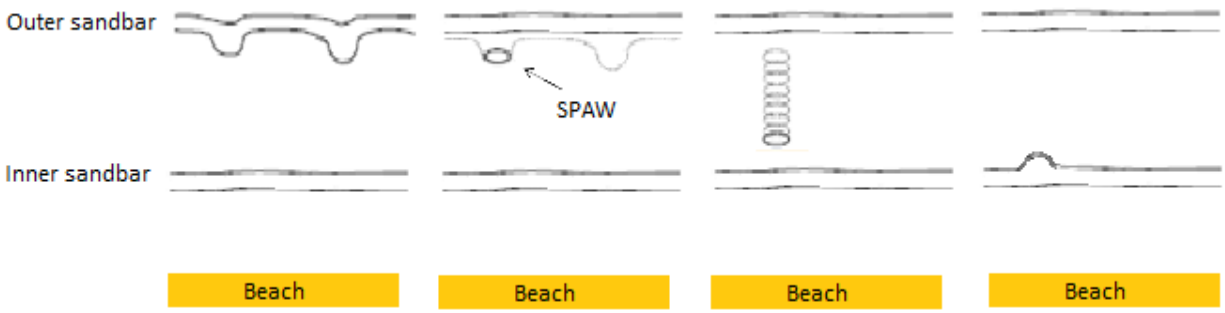

Figure 4 Conceptual sketch of SPAW initiation and migration designed by Van der Weerd (2012), adapted by De Wit (2016). Visible are beach, inner bar, outer bar and SPAW. Well-developed crescentic bar (a), followed by the formation of the SPAW (b). The SPAW migrates towards the inner sandbar (c) and subsequently merges with the inner sandbar (d).

Formation

The precise mechanism leading to SPAW formation is not well understood. However, observations have shown that SPAWs form during high energetic conditions, at sandbars with well-developed crescentic patterns where horns are almost welded with the inner sandbar (Almar et al., 2010; Wijnberg et al., 2010; Konicky and Holman, 2000; Van der Weerd, 2012). The definition SPAW is justified once the horn part of bar is separated from the main bar (Figure 4b) (Van der Weerd, 2012).

Migration

Once the SPAW is detached from the outer bar it migrates through the trough and eventually attaches to the inner sandbar (Figure 4). The onshore migration can be attributed to net onshore sediment transport over the SPAW; erosion on the seaward side and sedimentation on the landward side of the SPAW (Figure 5) (Van der Weerd, 2012). The underlying processes will be elaborated on in section 2.3.3.

Table 1 Overview of the locations including its characteristics where SPAWs have been observed.

Sites	Slope	Environment	Bar system	Sediment sand	Average wave height/period
Palm Beach	1:50	Swell	One	Medium	1.6 m / 10 s
Duck	1:12.5	Swell	One or two	Medium	1 m / 8 s
Le TrucVert	1:20	Wave	Two	Medium	1.4 m / 6.5 s
Agate Beach	1:70	Swell	Triple	Medium	2 m / 11 s
Egmond aan Zee	1:30 - 1:50	Wave	Triple	Medium	1.2 m / 5 s

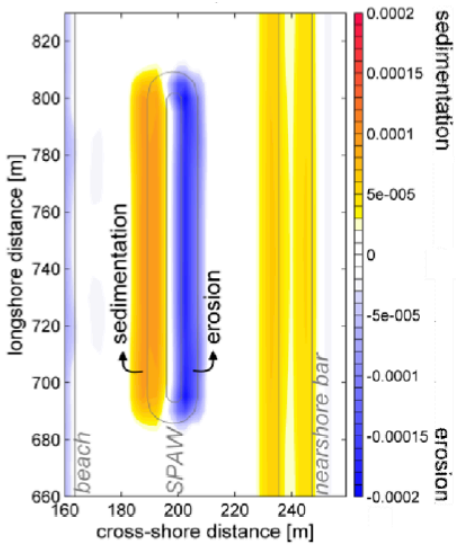

Figure 5 As designed by van der Weerd (2012) a topview of erosion-sedimentation pattern over SPAW.

Decay

Once the SPAW has moved through the trough the feature merges with the beach or the inner sandbar (Figure 4d). The volume of sand from the SPAW is being naturally spread out over the beach, the dunes or along the inner sandbar in the direction of the along shore current. Over time no more remnants are visible at the initial welding location (Wijnberg et al., 2007; Van der Weerd, 2012).

2.3.2. SPAW Observations

SPAWs have been observed at many different locations in the past years; Palm Beach (USA), Duck (USA), Le Truc Vert (France), Agate Beach (USA) and Egmond aan Zee (Netherlands) (Table 1 **Overview of the locations including its characteristics where SPAWs have been observed.**. Le Truc Vert and Egmond aan Zee are multiple barred systems. At these locations the SPAWs were found to shed of from the outer bar an eventually merge with the inner bar. At Palm Beach, Duck and Agate beach the SPAW was shed of from the bar and merged with the beach (Van der Weerd, 2012). Albeit the very different hydrodynamic and morphodynamic behaviour, SPAWs were observed, indicating that SPAWs are part of standard nearshore processes.

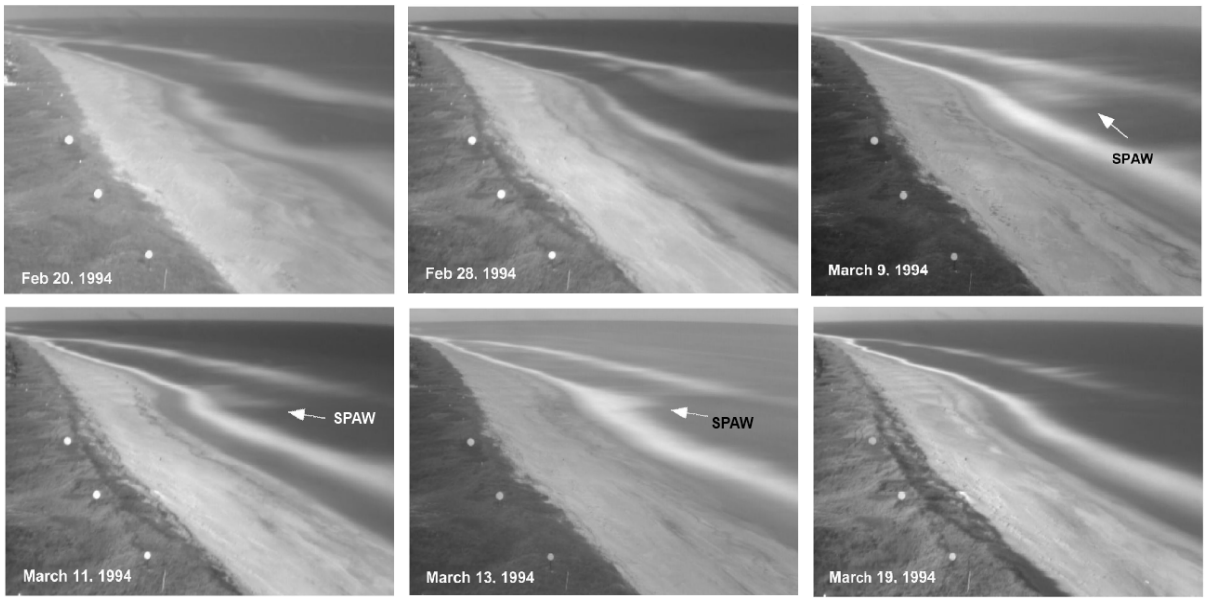

Figure 6 Sequence of time-exposure images near Duck illustrating a SPAW event (Wijnberg and Holman, 2007).

Three observational studies on SPAWs were carried out and provide written information: Duck (Wijnberg and Holman, 2007), Le Truc Vert (Almar et al., 2010) and Egmond aan Zee (Van Kuik, 2016).

The SPAWs at Duck and Le Truc Vert have been observed by scanning trough long series of time-exposure images by eye by multiple people independently (Wijnberg and Holman, 2008; Almar et al., 2010, respectively). The time-exposure images for Egmond aan Zee were

scanned for SPAWs by only one individual (Van Kuik, 2016). The presence of an isolated patch of foam in between the outer sandbar and the inner sandbar of the beach indicates a local subtidal feature: the SPAW (Figure 6b,c,d). Once the SPAW is recognized the start and end date are determined. The start date of the SPAW is defined as the first day on which the separation of the SPAW from the sandbar can be recognized (Figure 6c). The ending date of a SPAW is defined as the day at which no recognizable remnants are at the inner bar or the beach (Figure 6f). The definitions of both the start date and the end date were first introduced by Wijnberg and Holman (2007) and taken over by Almar et al., (2010) and Van Kuik (2016). The three observation studies determined the SPAW size according to the width and the length of the foam patch, where the foam patch is a proxy measure for the actual size of the submerged feature (Figure 7) (Wijnberg and Holman, 2007; Almar et al. 2010; Van kuikk, 2016).

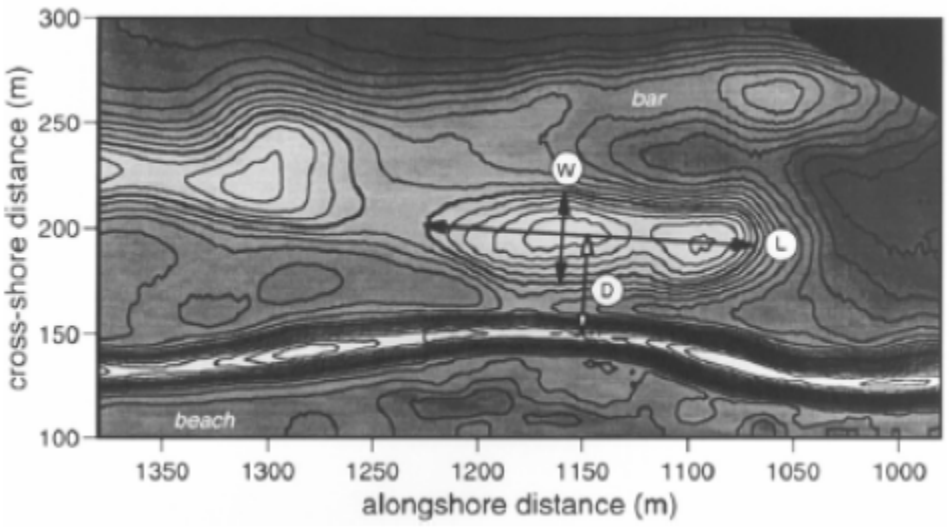

Figure 7 Definition sketch of morphometric measurements based on contoured time-exposure images (contours based on pixel intensity). W= width, L = length, D = initiation distance (Wijnberg and Holman, 2007).

2.3.3. Modelling SPAWs

Van der Weerd (2012) performed a modelling study on SPAW behaviour. The most important findings are summarized in this section.

2.3.3.1. Processes

Horizontal cell circulation and wave non-linearity were identified as important mechanisms underlying SPAW migration (Van der Weerd, 2012).

Horizontal cell circulation

When the SPAW has detached from the outer bar it affects the local wave field: wave height varies locally since waves break over the feature causing energy dissipation and reduction of wave height. Waves however do not break next to the feature. These local variations induce cross-shore and longshore gradients in radiation stress. Due to gradients in radiation stress local set up is generated, causing increase in mean water level in the onshore direction. As a result of the processes described above water levels vary both cross- and longshore around the SPAW, these water level variations generate currents. Around the SPAW tips a horizontal circulation pattern is formed, which is onshore directed over the crest and offshore directed around the SPAW (Figure 8) (Van der Weerd, 2012).

Wave non-linearity

As waves propagate over the SPAW wave skewness and asymmetry increase. This leads to an increase in onshore near bed-load transport in the direction of wave propagation. The wave asymmetry above the SPAW increased in the same order of magnitude as the bed-load transport increased, indicating that wave non-linearity is an important aspect of sediment transport over a SPAW (Van der Weerd, 2012).

The bedload transport was slightly directed towards the center of the SPAW, resembling the refraction pattern of the waves and not the horizontal cell circulation pattern. Therefore wave non-linearity is the driving force for increased onshore sediment transport and thus for the onshore migration of the SPAW (Van der Weerd, 2012).Which is the same process driving the onshore migration of sandbars.

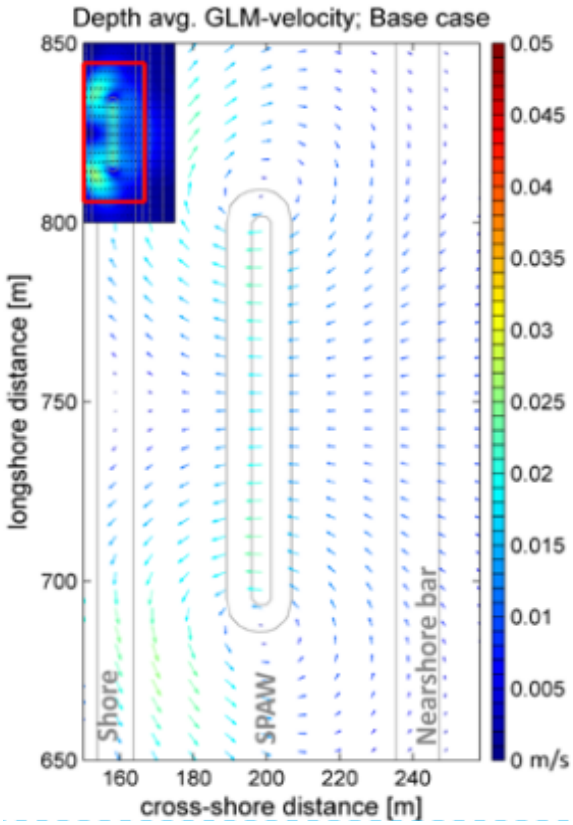

Figure 8 Top view of the depth averaged velocity patterns around the SPAW locations. Vectors show direction and magnitude, the colors indicate bathymetry (Van der Weerd, 2012).

2.3.3.2. Hydrological and morphometric variations

SPAWs have been observed at different locations with varying morphological and hydrological conditions. Van der Weerd (2012) found that the only variations influencing SPAW behavior were related to changes in SPAW width and changes of the surrounding bathymetry. A wider SPAW showed less sedimentation and erosion compared to the base case, indicating lower onshore migration rates for larger SPAWs. The surrounding bathymetry was changed by lowering the seaward sandbar. The study showed that the sediment transport over the SPAW increased and was directed onshore. The wave height of waves reaching the SPAW is higher for the scenario with a lower outer sandbar. This relatively high wave height resulted in stronger wave nonlinearity, leading to a stronger onshore-directed sediment transport.

2.3.4. Comparing literature

The SPAW event that were described in literature are compared in this section: Duck (Wijnberg and Holman, 2007), Le Truc Vert (Almar et al., 2010) and Egmond aan Zee (Van Kuik, 2016). At Duck 19 SPAW events were analyzed, at Le Truv Vert one SPAW event was analyzed and finally at Egmond aan Zee 59 SPAW events were analyzed. Furthermore, where possible, findings from the observational studies are compared to the modeling study by Van der Weerd (2012) and other studies addressing SPAW-like features.

Generation

All observational studies reported the presence of well-developed 3D bar geometries and intense wave forcing during SPAW formation, indicating that high waves and well developed outer bar crescents are the two factors dominating SPAW formation (Wijnberg and Holman, 2007; Almar et al., 2010; Van Kuik, 2016).

Shand (2007) studied a phenomenon very similar to a SPAW event. Bar-splitting involves a longshore bar developing a forked or bifurcated appearance with the seaward bifurcate migrating further offshore while the inner bifurcate moves into the landward trough and completely detaches from the original bar. This is the same mechanism as described by Almar et al. (2010), who found that, during a storm, the sandbar straightened and moved offshore, while part of the horn remained at its original location and formed the SPAW. Other than Shand (2007) and Almar et al. (2010), Van der Weerd (2012) proposed that, when wave conditions become more energetic, the three-dimensionality of the sandbar rapidly becomes linear, and in case onshore protruding part is separated from the main bar a SPAW is formed.

Migration

Wijnberg and Holman (2007) described that the SPAW dimensions remained the same during its onshore migration, and that the SPAW remained an intact feature at Duck. Almar et al. (2010) and Van Kuik (2016), however, found that at LTV and Egmond aan Zee the length of the SPAW decreased with 150 m and 66 m, respectively, during the onshore migration. Moreover the dimensions, the dimensions from the observational studies were used to compute the average SPAW volume for each location (Table 2). As the SPAW height for Egmond aan Zee was not available, for this case the average height from Duck was used, as these SPAW events resemble each other most. The average SPAW volume for Egmond

aan Zee, Duck and LTV were, 2700m3, 7000m3 and 1500m3 respectively. The SPAW at LTV clearly presents the largest volume. This large volume might be linked to the strong crescentic pattern and the large wavelength of the sandbar system at LTV compared to Duck. The sandbar system at Egmond aan Zee, however, also shows large wavelengths and strong crescentic patterns compared to Duck (Table 2). As such, the relation between sandbar characteristics and SPAW volume is false, or the volume computation for Egmond aan Zee is not correct.

The time the SPAW needed to transit the trough varies significantly for the three cases. At TVB the SPAW only needed a day to transit the trough (Almar et al., 2010), near Duck SPAWs took an average of 17 days (Wijnberg and Holman, 2007), and near Egmond aan Zee, Van Kuik (2016) determined the average time a SPAW needed to transit the trough was 38 days. Almar et al., (2010) linked the difference in transit time to wave action and crescentic bar development based on one SPAW observation at TVB compared to 19 SPAW observations at Duck. As for LTV just one event was analysed, it is hard to make a comparison. Therefore the hypothesis concerning the wave action of Almar et al., (2010) with data from Duck and Egmond was tested. The second link Almar et al., *(2010)* proposed (crescentic bar development) involves the distance a SPAW needs to overcome. When the horns of the bar are developed in the trough the distance decreases, hence the time the SPAW needs to transit the trough also decreases. To take the distance out of the equation a comparison according to migration rates per day was made. The average SPAW migration rate at Egmond is 1.36 m/day compared to 3 m/day at Duck (Van Kuik, 2016 and Wijnberg and Holman 2007, respectively). These migration rates contradict the hypothesis formulated by Almar et al., (2010). In a modelling study Van der Weerd (2012) found no relation between wave height and propagation speed over the lifetime of a SPAW. To be able to confirm or reject the model findings of Van der Weerd (2012) more long-term averages concerning migrations rates should be determined.

Table 2 Overview of conditions at three different beaches (Castelle *et al.*, 2003[2]; Almar *et al.*, 2010[1]; Howd and Birkemeijer, 1987[3]; Wijnberg and Holman, 2007[4]; Ruessink *et al.*, 2000[5]; Van Kuik, 2016[6])

	LTV	DUCK	Egmond aan Zee
Environment	Wave[1]	Swell[3]	Wave[5]
Bar system	Double[1]	Single/Double[3]	Triple[5]
Slope	1:20[1]	1:12.5[3]	1:30[5]
H_{rms} [m]	1.4[1]	1.0 [3]	1.2[5]
A [m]	75[1]	2-30[3]	5-40[5]
Tide [m]	1.5-4.5[1]	1-1.3[3]	1.3-1.6[5]
L [m]	600[1]	250[3]	575[5]
Observed SPAWs	*1*	*19*	*57*
SPAW Length [m]	*100:250[2]*	*126 +/- 60[4]*	*218[6]*
SPAW Width [m]	*72[2]*	*30 +/- 10[4]*	*31[6]*
SPAW Height [m]	*Mean 0.7; Max 1.0[2]*	*Mean 0.5[4]*	-
Trough transit time [days]	*1[2]*	*17[4]*	*38[6]*

2.3.5. Research Gap

Currently SPAWs are being detected by visually scanning through years of time-series of time-exposure images. Even though multiple individuals perform the scanning separately, there might still be a risk of subjectivity. Furthermore, the width and length of SPAWs are being determined from the size of the foam patch resulting from depth induced wave breaking over a SPAW. The size of the foam patch however does not only depend of the width and length of the SPAW, but is also influenced by wave conditions. During energetic wave events the wave breaking over a SPAW becomes more intense, resulting in a large foam patch. During low energetic wave conditions wave breaking over a SPAW will be less intense, resulting in a small foam patch. Also waves might not even break, making the feature absent in the time-exposure image. Regardless, the size of the foam patch does not always correlate with the size of the SPAW. Finally, the average height of a SPAW was determined to be 0.7m by Wijnberg and Holman (2007) by a one-time bathymetric survey. The volume of SPAW features subsequently has been calculated using a height of 0.7 meters.

Considering that this height can only be confirmed by one bathymetric survey this value is not reliable. To be able to calculate the volume more accurately more bathymetric surveys should be performed. However, given the non-periodic behavior of SPAW occurrences this might be a challenge.

A possibility is using an assimilation model to estimate the bathymetry based on video-derived observations of wave roller dissipation and intertidal bathymetry (Van Dongeren et al., 2008). Subsequent to the estimations of the bathymetry, the volume of a SPAW can be calculated.

2.4. Research questions

The first aim of this research is to develop an objective method to determine the presence of SPAWs and the dimensions of its features through time and space. The second aim is improving the understanding of the process by which the SPAW in its initial phase detaches from the outer bar and moves through the trough before attaching to the inner sandbar.

1) How can SPAWs be objectively derived from time-exposure video images?

a) What are suitable features to objectively extract SPAWs from the images?

2) How can the SPAWs dimensions objectively be extracted from the bathymetric maps?

a) Is it possible to quantify SPAW depth, height and volume from the images?

3) What is the temporal and spatial variation of natural SPAW dynamics?

a) How do characteristic SPAW properties vary in space and time?

b) What are the boundary conditions (bar state, waves) during SPAW generation, onshore migration and decay, respectively?

2.5. Outline

Information on the study area and the data collection is described in chapter 3. Followed by a description of the steps that were taken to objectively derive a SPAW feature from GPV images, integrate the SPAW in the computation of bathymetric maps during the study period, and subsequently extract SPAW dimensions from the bathymetric maps (chapter 4). In chapter 5 the bathymetric maps are described and the SPAW dimensions over time in

combination with wave conditions are analyzed. Then the functioning of the assimilation model according to the results, and the results in relation to previous research is discussed in Chapter 6. Finally the conclusions and future recommendations are presented in chapter 7.

3. Study area and data collection

3.1. Study area

The SPAW dynamics were studied near the beach of Egmond aan Zee, The Neterhlands, located at the central part of the Dutch coast (Figure 9). The exact location of the study site is in between beach pole 41.25 and 39.25 (red dots in Figure 9). The coast of Egmond aan Zee is approximately north-south orientated and experiences a semi-diurnal tide with a 1.4 m and 2.1 m tidal range during neap and spring tide, respectively. Waves predominantly approach the shore from south-westerly and north-westerly directions. The yearly averaged significant offshore wave height is about 1.2 m, with a mean period of 5 s (Aagaard et al., 2004; Van Dongeren et al., 2008). The wave height can reach up to 5.0 m during storms, especially when the waves are incident from the north-west (Price & Ruessink, 2008). Two sub-tidal sandbars and one intertidal sandbar dominate the nearshore bathymetry.

The outer subtidal bar is straight with occasional long-shore irregularities with periods exceeding 1 km (Short, 1992). The location at which this sandbar is located is approximately 5 m deep; as such waves rarely break on this feature. The inner subtidal sandbar is often characterized by significant quasi-periodic alongshore variations with a longshore wavelength varying between 350 and 900m (Short, 1992). The intertidal sandbar also shows significant quasi-periodic alongshore variations, however the wavelength of these features is often slightly smaller than that of the inner subtidal sandbar.

The most outer subtidal sandbar is not included in this research, motivated by the lack of wave breaking over the bar, further discussed in section 3.2.1. As such, the inner subtidal sandbar will be denoted as the outer bar and the intertidal sandbar will be denoted as the inner bar.

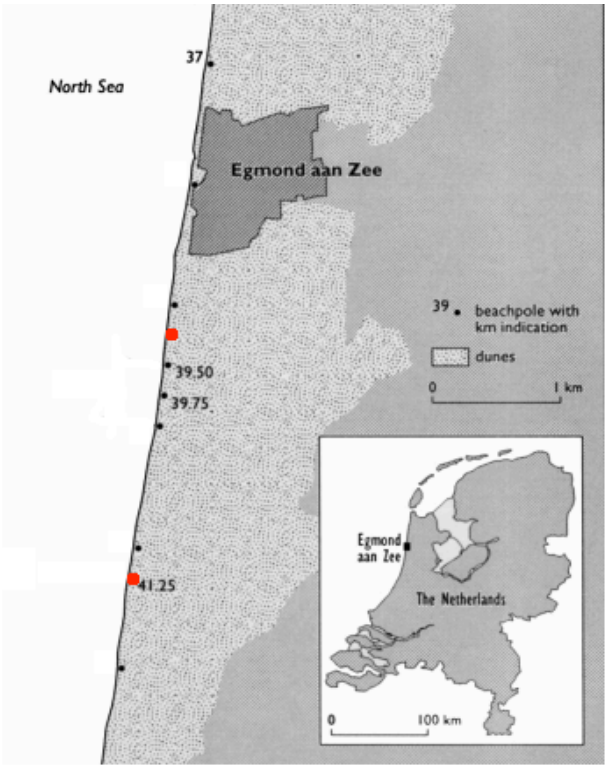

Figure 9 Overview of the study site, where the red dots indicate the alongshore extend of the research area.

3.2. Data Collection

For this study a SPAW event between 09-07-2001 and 07-09-2001 was examined, henceforth referred to as the study period. The dataset consists of coastal Argus images and offshore wave conditions during the study period and an initial bathymetric profile, the three data sources are discussed separately in subsections 3.2.1, 3.2.2 and 3.2.3, respectively.

3.2.1. Video Imaging

In 1986 the Oregon Imaging lab created the Argus program, a coastal imaging system, and now, 30 years later, all over the world Argus stations are in operation. Between 1999 and 2014 Argus gathered images of the nearshore coastal area near Egmond aan zee. For this study the available images during the study period were extracted from the database. The Argus system near Egmond aan Zee physically consists of five cameras installed at an elevation of 48 m above mean sea level, on a tower located near the dune foot at beach pole 41.25, providing 180˚ uninterrupted coverage of the coast. Each daylight hour the system routinely collected a 10min time-exposure image for every camera (Holman and Stanley, 2007). Moving features such as waves are averaged out and only their mean brightness

returns (Holman and Stanley, 2007). The time-exposure images where rectified and merged to obtain planview images with coverage of 4000m in longshore direction and 1200m in cross-shore direction. Concerning the cross-shore extent of the cameras only the most shoreward 800m were used, motivated by the lack of breaking waves in the remaining part of the image. From the alongshore extent only the most northern 2000m in range of the cameras was selected (camera 1 and 2), motivated by frequent lack of quality in the remaining reach of the cameras due to sunglare, and the presence of the SPAW event in that specific area. During the study period in total 1914 time-exposure-images from camera 1 and 2 were extracted from the Argus database and merged into 957 planview images. The planview images captured the SPAW event, which is described in detail section 3.2.2. Furthermore, the planviews, displayed in RGB, were converted to grayscale planviews (GPV) by eliminating the hue and saturation information while retaining the luminance (Figure 10) (Matlab, 2016).

Crest lines of the inner[1] and outer[1] sandbar and the shoreline were extracted from one time planview each day by the automated alongshore tracking of intensity maxima across each bar and shoreline (Figure 11) (Pape et al., 2010). To minimize the barline variability related to changes in tidal water level, only low-tide images were used (Van Enckevort and Ruessink, 2001; Pape et al., 2010). Due to an applied smoothing factor in the alongshore tracking of the intensity maxima the tracked intensities did not always exactly match the real alongshore-maximum intensities.

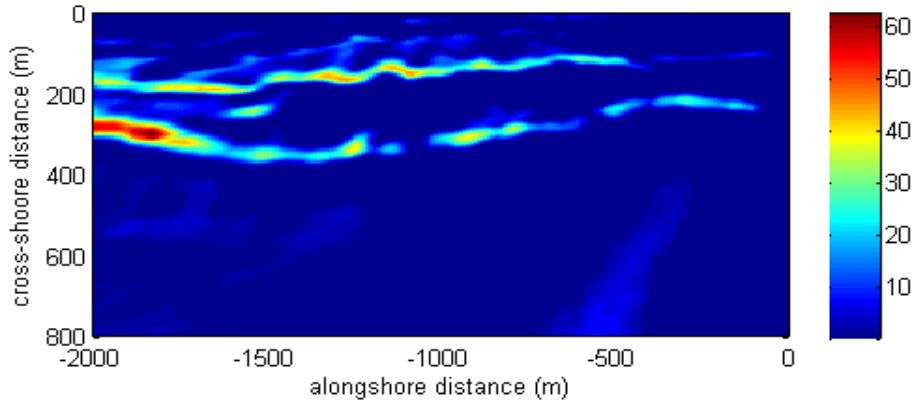

Figure 10 Gray scale planview with x = alongshore distance and y = cross-shore distance, with 0 being the beach, and 800 being 800 m offshore.

[1] Terminology as introduced in section 3.2 (p. 28).

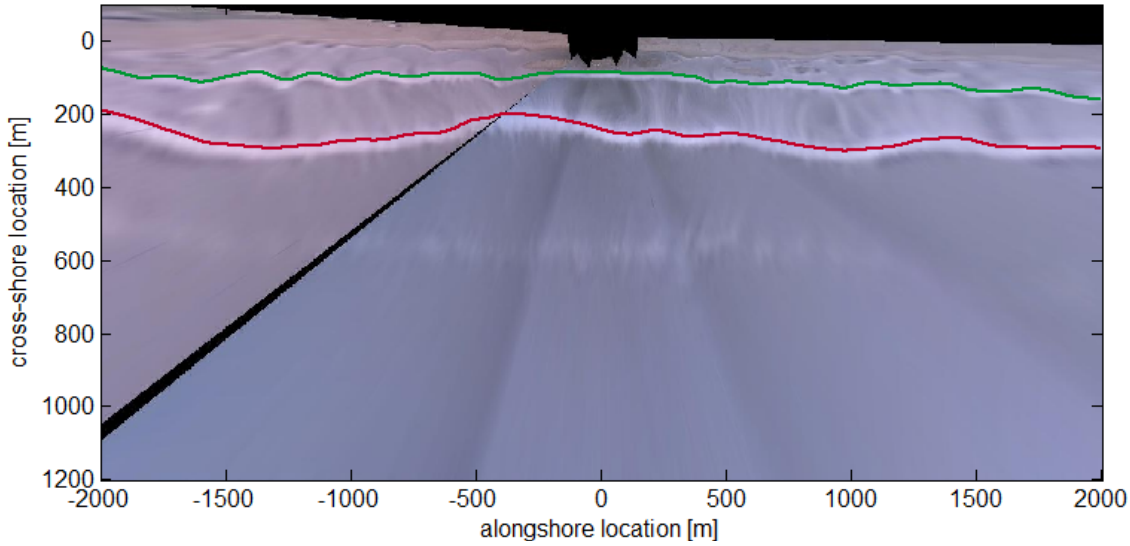

Figure 11 Example of 5 merged Argus images at 03-08-2001 GMT 15.00 with the crest lines of the inner (green) and the outer (red) sandbars.

3.2.2. Wave and tide data

During the study period hourly offshore root-mean-square wave height (H_{rms}), peak period (T_p) and angle of incidence with reference to shore normal (θ) (Figure 12a, b, c, respectively), were measured hourly with a directional wave buoy located approximately 40 km offshore from the study site at a water depth of approximately 25 m (Aarninkhof et al., 2005).

Wave events can be identified by means of the wave power P (Figure 12d). Short (1979) identified (P), which incorporates both H_{rms} and Tp, as an important parameter governing morphological changes.

$$P = \frac{\rho g^2}{32\pi} H^2{}_{rms} T_p \quad (4)$$

The alongshore components of the wave power P_y (Figure 12e) was computed to analyse the effect of θ at the study site. P_y represents the portion of the wave power available for alongshore sediment transport.

$$P_y = P \sin\theta \cos\theta \quad (5)$$

During the study period the variations in H_{rms} are dominant over the variations in T_p, as such the results are analyzed according to H_{rms} and P_y.

The average H_{rms} during the study period was 0.35 m, this is low compared to the yearly averaged significant offshore wave height of about 1.2 m. Therefore, in this study high waves are defined as H_{rms} > 0.7 m and low waves are defined as H_{rms} < 0.3 m.

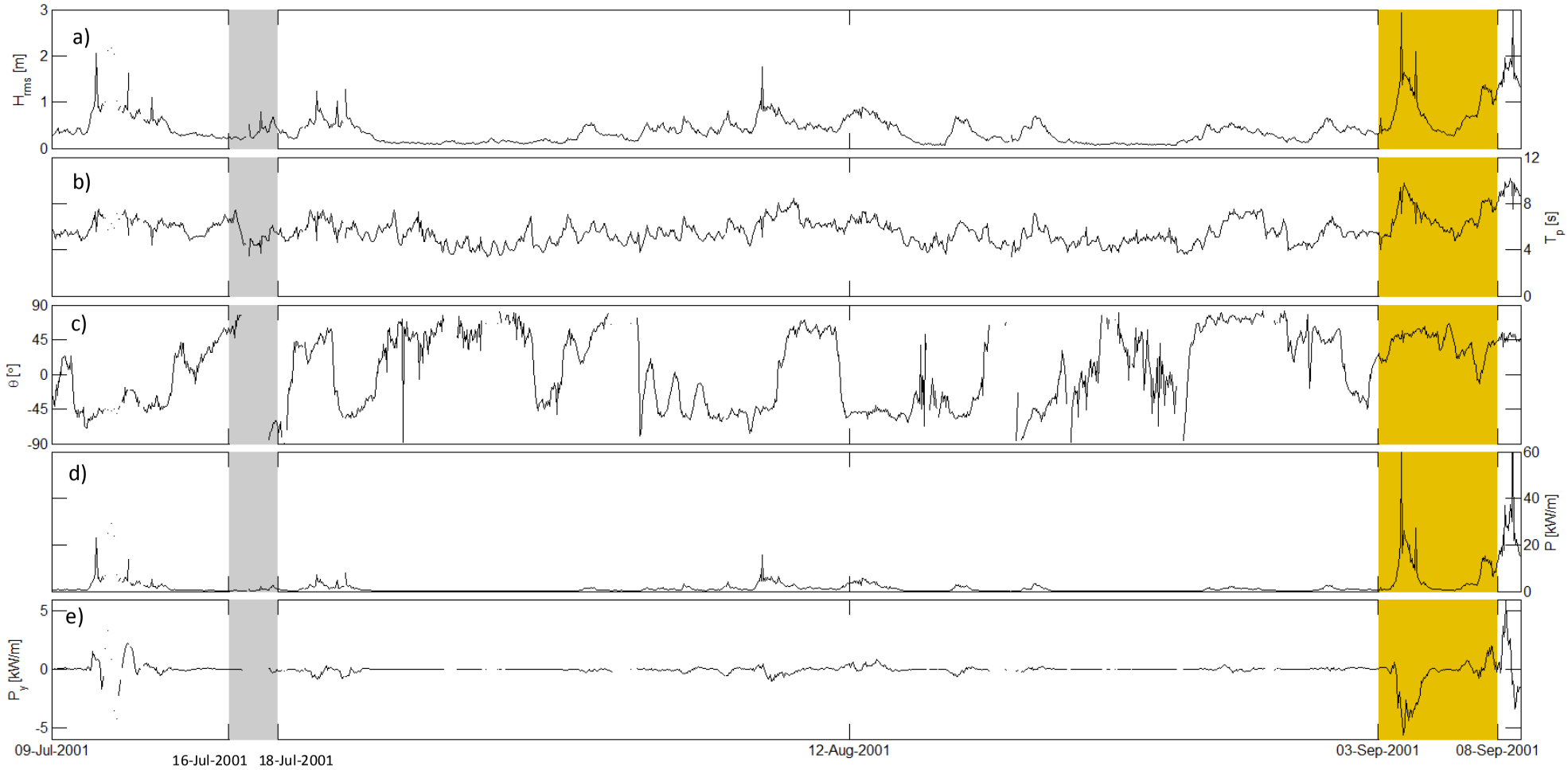

Figure 12 (a) Hourly root mean square wave height (H_{rms}), (b) peak period (T_p), (c) angle of incidence with reference to the north (Θ), (d) wave power (P) and (e) alongshore wave power (P_y) between 09-07-2001 and 07-09-2001. The grey box indicated the period during which the SPAW detached from the outer sandbar, and the gold box indicates the period during which the SPAW merged with the inner sandbar, these periods are based on the SPAW event in the time-exposure images.

SPAW event according to planview images

On the basis of planview images and wave data during the study period the SPAW event is described. Between 1 July and 9 July the waves were low (H_{rms} < 0.5m). After this period of calm weather, the outer bar showed a clear landward protruding horn (Figure 13a). After 10 July the wave height increased to 2 m, which coincided with the seaward migration of the sandbar. Not the whole sandbar migrated seaward, part of the horn remained at its original location, still connected to the seaward sandbar (Figure 13b). 18 July is the first day at which the SPAW is visible as being detached from the outer sandbar (Figure 13c), the detachment did not coincide with high waves. Time-exposure images before 18 July also show the SPAW, however, in these images the outer sandbar is not visible, subsequently the SPAW might have detached from the outer sandbar between 16 July and 18 July (grey box in Figure 12). After the detachment, the SPAW remained in the trough between the inner and the outer sandbar for more than a month, 18 July until 3 September (Figure 13e). On 4 September and 5 wave height increased up to 3 m, the energetic wave breaking caused residual foam, this made it hard to distinguish the SPAW. On 8 September the planview image shows the outer- and inner sandbar, no more remnants of the SPAW are visible, indicating that the SPAW merged with the inner sandbar between 3 September and 8 September, when waves were high (gold box in Figure 12, Figure 13f). The distance between the inner and the outer bar, which the SPAW transited, was approximately 180 m.

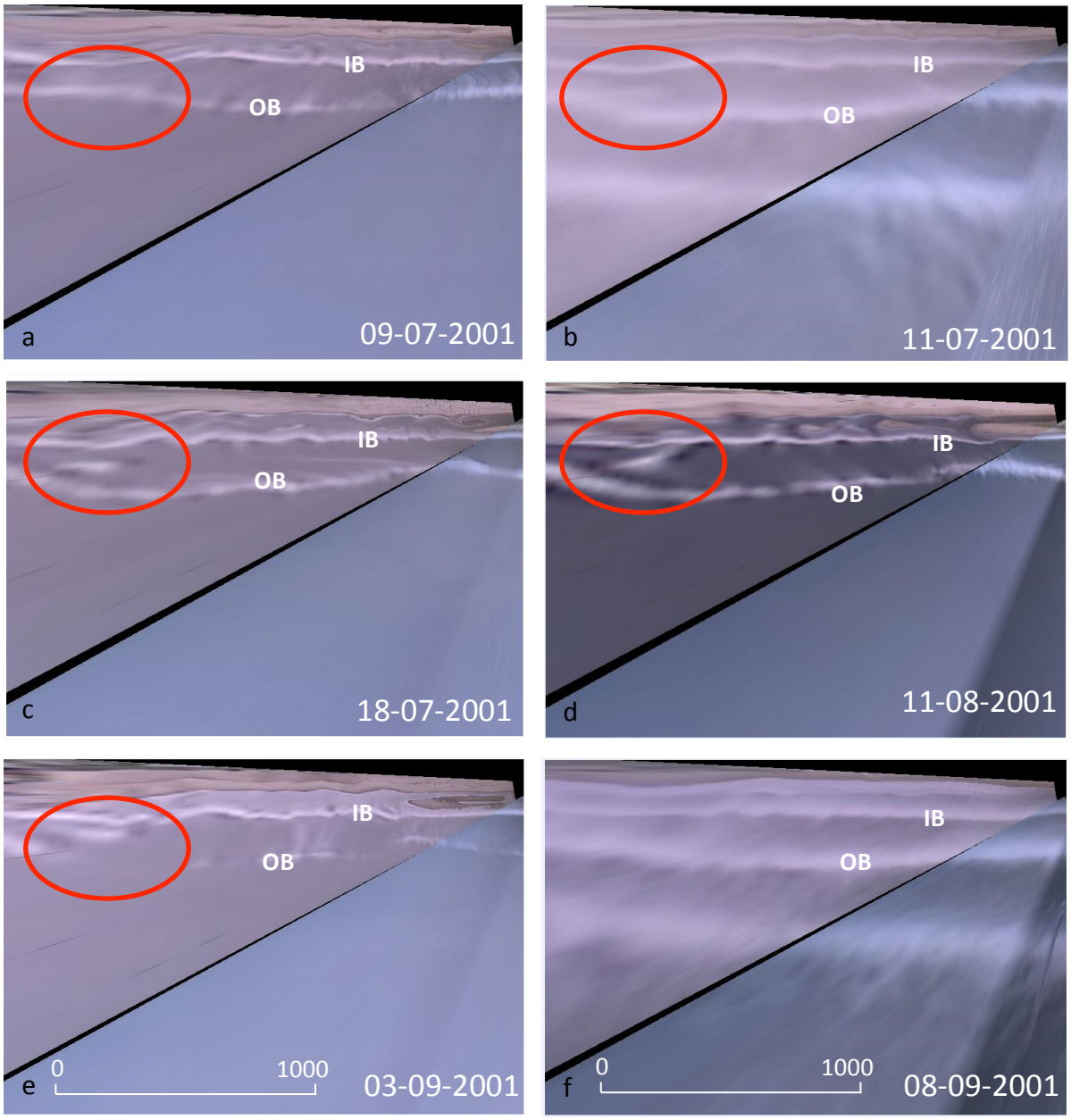

Figure 13 Planview images during the SPAW event (a) on 09.07-2001 with a well-developed outer sandbar, (b) on 11-07-2001 where the outer sandbar migrated offshore and the horn remained at the same location, (c) on 18-07-2001 with an islotated foam patch, indicating that the SPAW detached, (d) on 11-08-2001, showing the SPAW, (e) on 03-09-2001, where the SPAW is almost welded to the inner sandbar and (f) at 08-09-2001, no more remnants of the SPAW are visible, SPAW has welded to the beach. The red circles indicate the area of interest, and IB stands for outer bar and IB stands for inner bar. The scale in (e) and (d) apply for all subfigures.

3.2.3. Bathymetric data

The initial bathymetric profile measured on 25 July 2001 was obtained from the Jarkus (JAarlijkse KUStmeting) database of Rijkswaterstaat. The date of this measurement was closest to the first date of the study period (09-07-2001). The initial resolution of the Jarkus profile was 250 m alongshore and 20 m cross-shore. To improve the resolution of the bathymetric Jarkus profile a Loess interpolation was performed giving a final resolution of 10 m alongshore and 5 m cross-shore (Figure 14). The low resolution of the JarKus profile resulted in the absence of nuanced features, such as a SPAW in the bathymetric map.

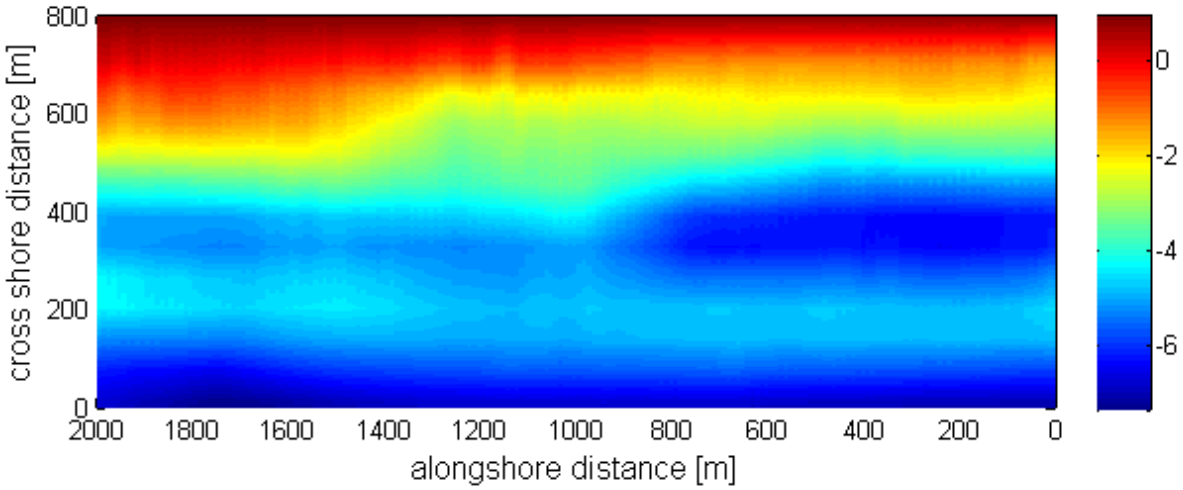

Figure 14 Initial bathymetric profile as extracted from the Jarkus Database.The colorbar indicates the elevation. Interpolated to a resolution of 5 m cross-shore and 10 m alongshore.

4. Generate Bathymetric maps

Bright white bands or patches on planview images give an indication of the subtidal bathymetry during the study period. However, exact measures on features such as sandbars and SPAWs can't be extracted from planview images. To analyze the SPAW dimensions over time bathymetric maps during the study period are needed.

In 2005 Aarninkhof et al., (2005) presented an assimilation model where time-exposure images were used to estimate cross-shore bathymetry. The technique is based on the linear relationship between accretion and erosion, and the difference between modelled and observed wave roller dissipation. Van Dongeren et al., (2008) improved the assimilation model by Aarninkhof et al. (2005) by extending the number of remote-sensing data sources, and reduce the number of free parameters relative to Aarninkhof et al. (2005).

The bathymetry during the study period can be estimated based on the data sources described in section 3.2. Practically, several steps needed to be taken to prepare this data and to compute bathymetric maps during the study period. First all time-exposure images during the study period were transformed into intensity maps (imaps). Subsequently the imaps and the wavedata (H_{rms} and θ) were used to compute the D_r, which describes the energy of wave dissipation. Finally an initial bathymetric map at t=x-1 and a D_r map at t=x are used to compute a new bathymetric map at t=x (Figure 15).

This chapter aims to describe the steps that were taken to objectively derive a SPAW feature from GPV images, integrate the SPAW in the computation of bathymetric maps during the study period, and subsequently extract SPAW dimensions from the bathymetric maps.

The process of computing bathymetric maps during the study period comprises data preparation (section 4.1) and the assimilation process (section 4.2). Finally in section 4.3 the methods to extract the SPAW dimensions from the bathymetric maps are described.

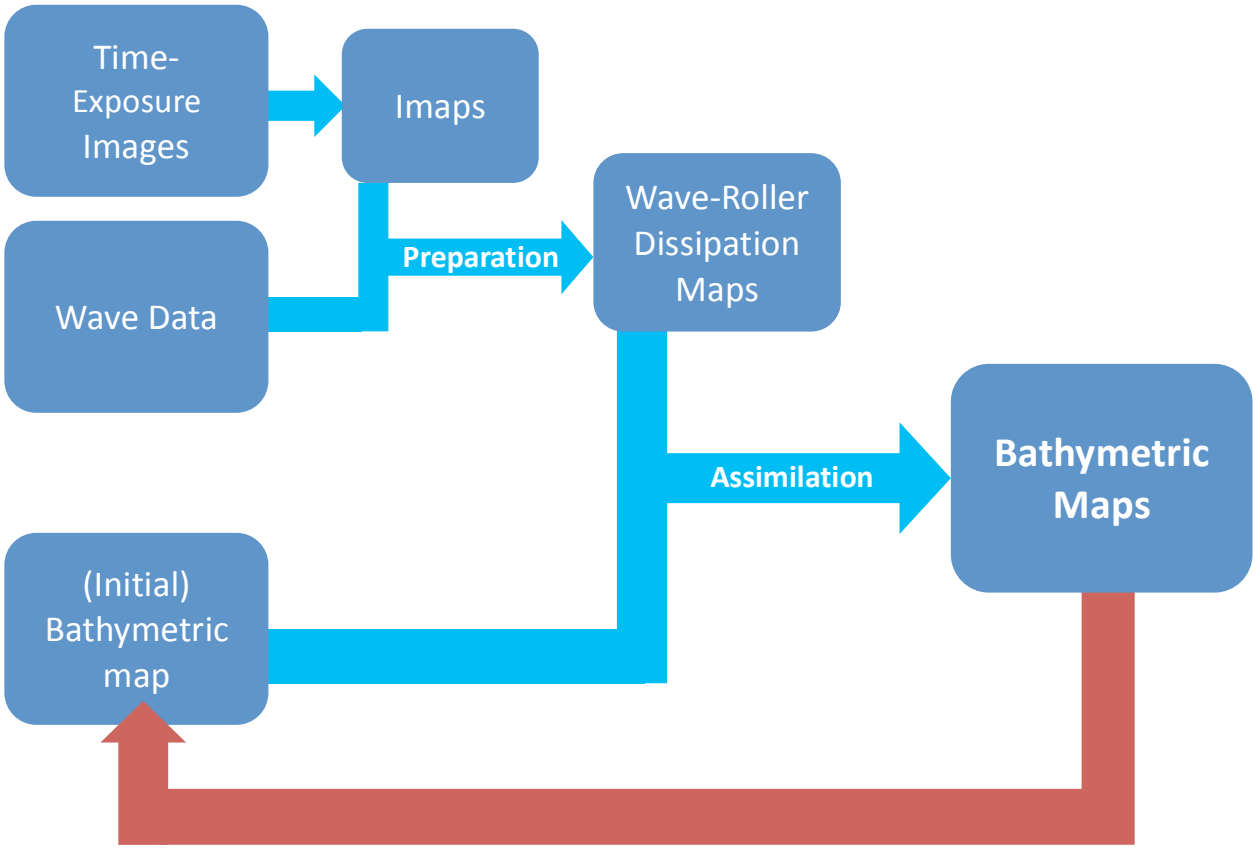

Figure 15 Schematic overview of the practical steps that need to be taken to compute bathymetric maps from time-exposure images, wave data and an (initial) bathymetric map.

4.1. Data preparation

4.1.1. Extract roller dissipation from time-exposure images

In the ideal case roller dissipation (D_r), variations in intertidal shoreline and wave celerity (c) would be available to estimate bathymetry. However, for this study the only available source of input for the assimilation model was D_r.

For the quantification of D_r from the video images the methods developed by Aarninkhof and Ruessink (2004) were broadly followed.

Firstly, individual time-exposure images were transformed to geometrically correct plan views on a local coordinate system, such that that the barlines, and the alongshore axis of the image were approximately parallel to the shore (Figure 11). Secondly, offshore areas where no wave breaking takes place should correspond to zero intensity, therefore the

average background illumination (I_0) was removed from time-exposure image (Figure 16). I_0 is defined as the average intensity in the offshore region where during the study period waves never broke (red box in **Figure 16**a).

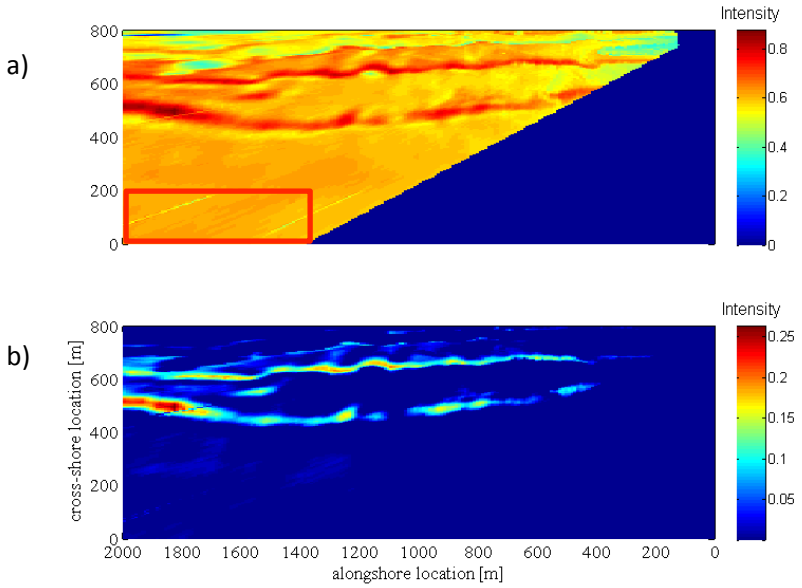

Figure 16 GPV from camera 1 on 09-08 GMT 14.00 with background illumination (a) and without background illumination (b). (a) The red box indicates the area of which the average background illumination (I_0) was computed. Note difference scales in colorbar.

Thirdly, the technique created by Alexander and Holman (2004) was used to remove noise from the GPV to create an observed wave roller dissipation map, or imap. Each cross-shore intensity profile is described in terms of an I_0, m_1 and $G(x)$ for each intensity peak:

$$G(x) = A_G \cdot e^{-\left(\frac{x-\mu_G}{\sigma_G}\right)^2} \quad (6)$$

where A_G, μ_G and σ_G are measures for height, mean location and width of a dissipation peak, respectively. Price and Ruessink (2012) adapted the technique by Aarninkhof and Ruessink (2004) such that the locations of μ_G of dissipation peaks were predefined and coincided with the position of the extracted barlines. In section 3.2.1 was described that the tracked alongshore-maximum intensity does not always match the actual alongshore-

maximum intensity. For each alongshore position, the locations of the automatically tracked maxima in the GPV (red circles in Figure 17b), were used to determine new maxima (green circles in Figure 17b). As such the following Gaussian approximation $\mathrm{I_G}$ of the video-based cross-shore intensity profile was formulated:

$$I_G(x) = I_0 + m_1 \cdot x + G_i(x) + G_o(x) \tag{7}$$

where $G_i(x)$ and $G_o(x)$ are Gaussian curves describing the dissipation peak over the inner and outer bar, respectively. For each intensity profile, I_0, m_1, and $A_G$and σ_G for each bar were computed using nonlinear least-squares data fitting with the Gauss–Newton method. With exclusion of I_0 and $m_1(x)$ the observed wave roller dissipation I_b of I_G (Figure 17a, b) is given by the following equation:

$$I_b(x) = G_i(x) + G_o(x) \tag{8}$$

With the methods developed by Aarninkhof and Ruessink (2004), Alexander and Holman (2004) and Price and Ruessink (2012) $I_b(x)$ is defined by the Gaussian curve over the inner and the outer bar. For this study the SPAW should also be included in $I_G(x)$ and subsequently $I_b(x)$. Therefore, the Gaussian approximation I_G was adapted such that, if a SPAW would be present in a cross-shore profile from the GPV, this SPAW could be included in the Gaussian approximation.

The first step was to determine, for each cross-shore profile of each GPV, whether a SPAW was present between the inner and the outer sandbar. To find the SPAW in the GPV, each cross-section of each map was examined for peaks in between the locations of the inner and the outer sandbar, when peaks exceeded a threshold of 1 the adapted Gaussian approximation I_G of the video-based cross-shore intensity profile was used. The threshold of 1 was found by trial and error; values higher than 1 missed SPAWs and values lower than found unjustified SPAWs. The adapted equation for $I_G(x)$:

$$I_G(x) = I_0 + m_1 \cdot x + G_i(x) + G_0(x) + G_S(x) \tag{9}$$

where $G_S(x)$ is the Gaussian curve describing the dissipation peak over the SPAW. For each intensity profile with a SPAW, the coefficients I_0, m_1, and $A_G$and σ_G were computed using nonlinear least-squares data fitting with the Gauss–Newton method; in the calculation of the

coefficients the SPAW is also included. With exclusion of I_0 and $m_1(x)$ the wave breaking component I_b of I_G (Figure 17a, c) is now given by the following equation:

$$I_b(x) = G_i(x) + G_0(x) + G_S(x) \tag{10}$$

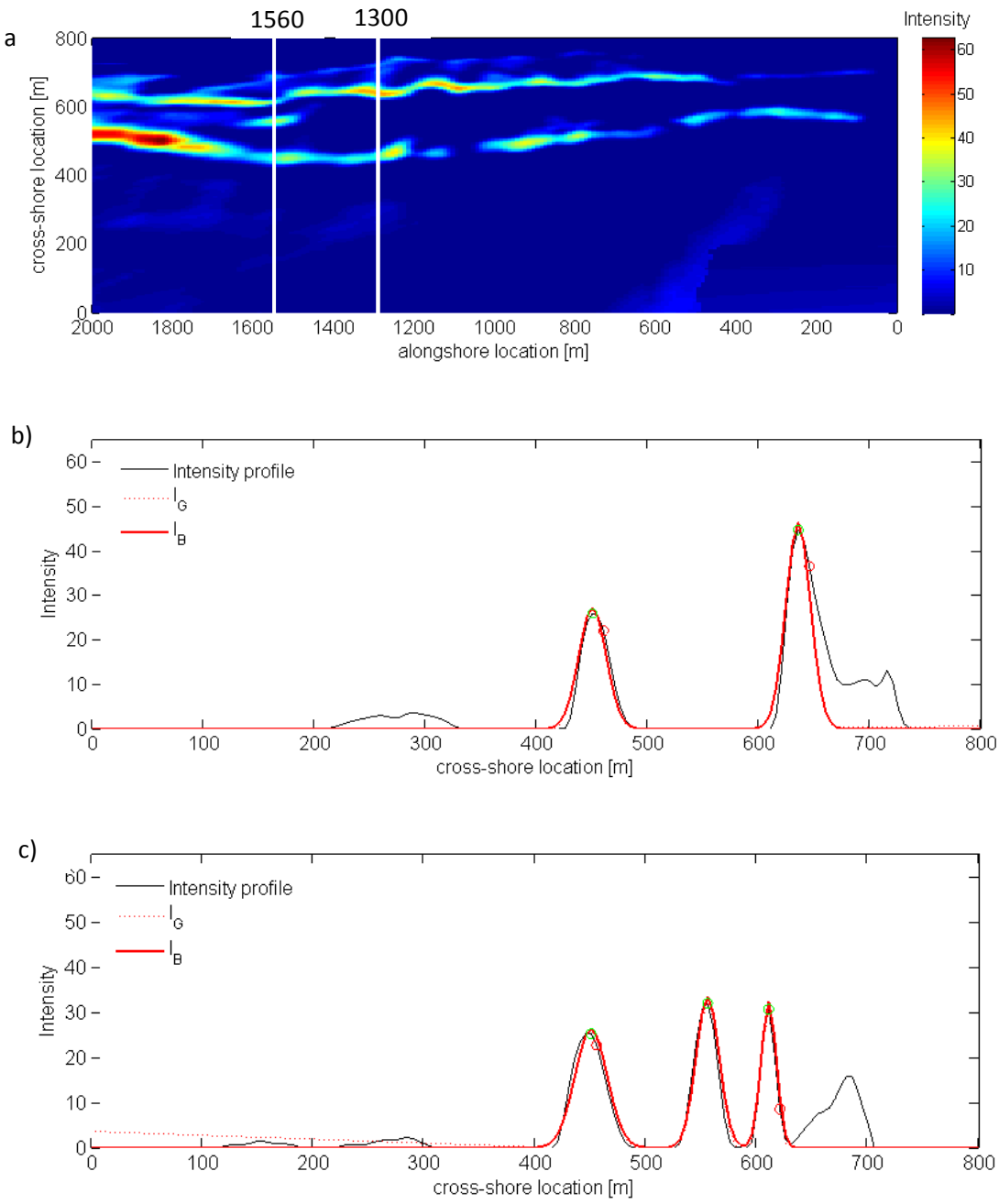

Figure 17 GPV (a) on 09-08-2001 GMT 14.00, where the white line indicates the cross section of interest. The intensity profiles for the cross-sections at x = 1300 (b) and a=1560 (d). In black the GPV cross-section, in red dashed I_G, and in red I_B. The green dots indicate the location of the outer bar and the inner bar. The red dots indicate the location of the bar crest lines extracted with the automated tracking of alongshore maxima.

The use of the threshold of 1 might have given subjective indications for the alongshore length of the SPAW. To correct for misidentified peaks between the inner and the outer sandbar another measure was taken; only when peaks in between the inner and the outer bar in five or more subsequent cross-sections exceeded the threshold the peaks was defined a SPAW (Figure 18). The cross-sections where is misidentification was recognized was refitted using Eq. (8) and Eq. (10). Even with this heuristic measure SPAW might have been misidentified. However, a careful comparison between the planviews and imaps showed that the main features in the planviews corresponded to the imaps.

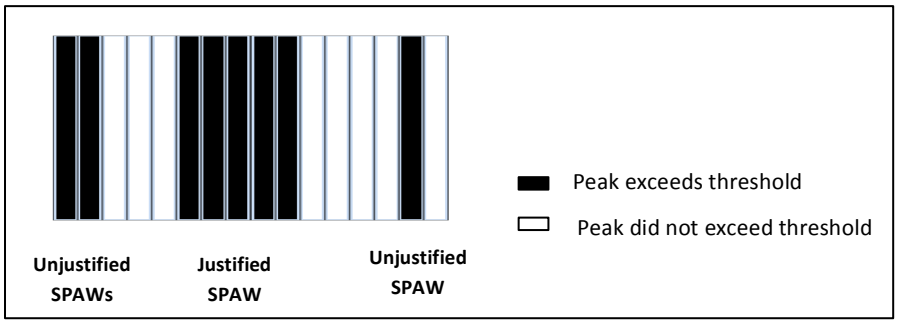

Figure 18 Schematic presentation of the final heuristic measure. In white the cross sections in which no SPAW was recognized and in black the sections in which a SPAW was recognized. With 5 or more subsequent recognized SPAWs the individual SPAWs are assumed true.

Fourthly, heuristic measures were taken in order to further improve the quality $\mathrm{I_b(x,y)}$ based on Eq. (7), Eq. (8), Eq. (9) and Eq. (10)

The computed I_0 and m_1 for each map in some instances presented with large fluctuations (Figure 19b, c, d, respectively), which could lead to an unrealistic D_r map. The fluctuations were considered outliers and removed by fitting a linear trend through the values. The linear trends trough the spiked I_0 and m_1 defined the new I_0 and m_1

Values for σ_G were found to be overestimated in some cases, therefore these overestimated values for σ_G were constrained by setting maximum values of $\sigma_{G,o,max} = 35, \sigma_{G,i,max} = 25$. These values were chosen after a careful examination of the dissipation peaks. Maximum values of 35 and 25 for the width of the dissipation peak over the outer- and inner bar, respectively, proved to yield to best results (Figure 19f).

In the cross-sections for which I_0 and m_1 and/or σ_G were redefined, $I_G(x)$ was refitted, resulting in an improved $I_b(x)$ (Figure 19e).

The Gauss-Newton method used to compute I_0, m_1, and $A_G$and σ_G was not always able to make a correct estimation within its number of preset iterations, which were 100. Increasing the number of iterations to 150 to improve fitting results did not outweigh the increased simulation time. For those cross-sections, in which the Gauss-Newton method failed to provide correct, I_0, m_1, and $A_G$and σ_G, were tracked, set to zero and interpolated (nearest neighbor); this may have caused $I_b(x, y)$ to be less accurate.

One of the reasons for the Gauss-Newton method not always being able to compute the correct coefficients might be linked to the extracted barlines defining the location of μ_G of the dissipation peak. When the location of the extracted barline was tracked inaccurately this led to an incorrect location of μ_G of the dissipation peak.

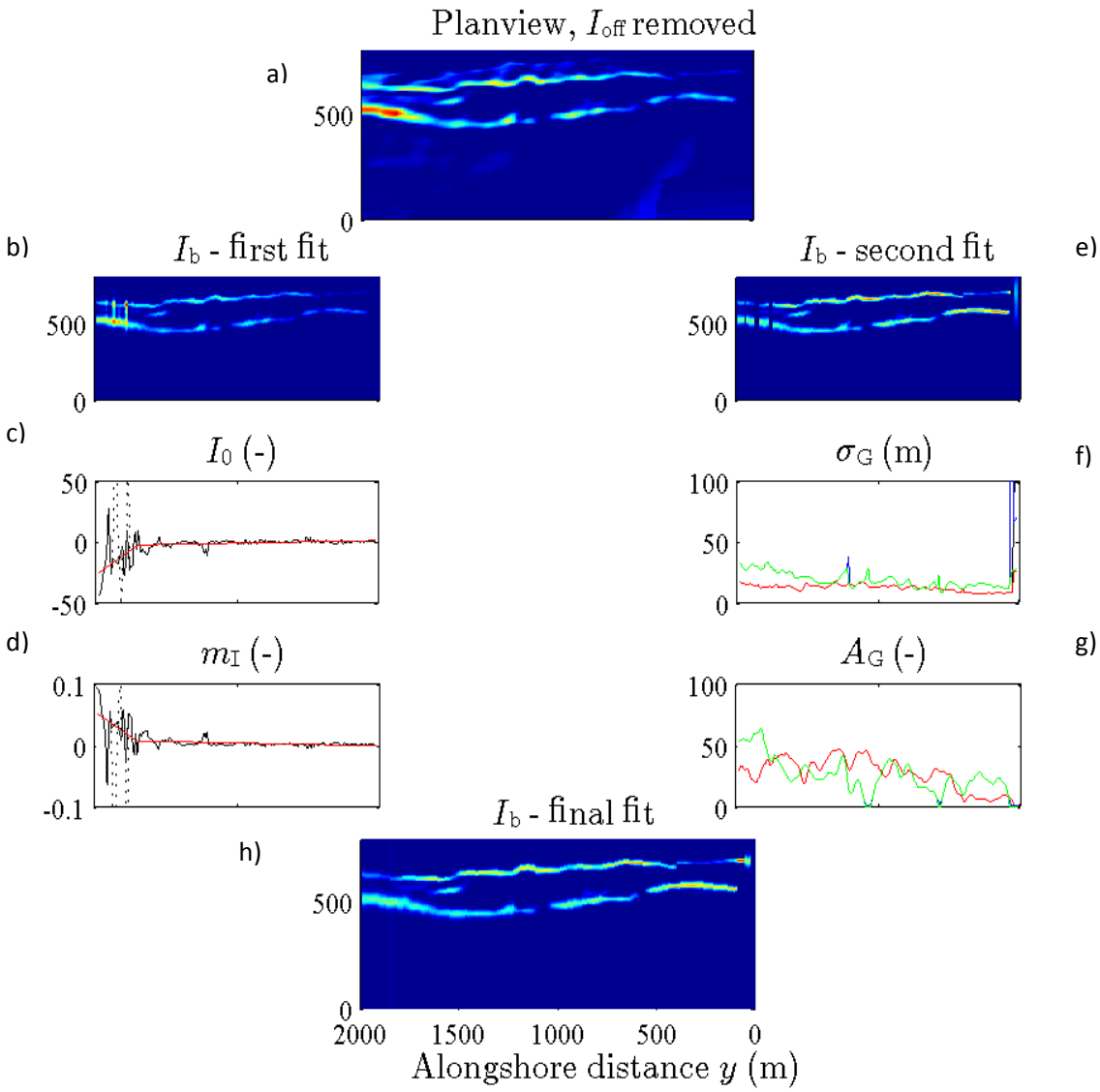

Figure 19 Example of image pre-processing, with (a) the rotated planview image from 09 August 2001 1400 GMT after removal of I_{off}, (b) the initial $\boldsymbol{I_b}$, (c,d) the linear fits (red solid line) applied to $\boldsymbol{I_0}$ and $\boldsymbol{m_1}$ (spiked, dashed black line), (e) the second $\boldsymbol{I_b}$, after applying the linear fits in (c) and (d), (f) $\boldsymbol{\sigma_{G_0}}$(red) and $\boldsymbol{\sigma_{G_i}}$(green) restraining the deviation in the inner and the outer bar, (g) $\boldsymbol{A_G}$ where possible outliers un the amplitude if the inner and the out bar are constrained, and finally (h) $\boldsymbol{I_b}$. In the intensity maps (a, b, e, h) the y-axis represent the cross-shore distance x (m), increasing towards the coast, the dark blue (bright red) colors in these maps correspond to 0 (maximum) intensity. The dotted lines in (c, d, f, g) represent non- despiked parameters.

Besides the barlines, the shorelines were tracked and used as a landward boundary condition, to prevent reflection from dry sand to be interpreted as wave breaking, shorelines were tracked and used as a landward boundary condition. The shorelines were tracked similar to the bar lines (automated longshore intensity tracking). However, due to unclear boundaries of the shorelines only few shorelines could be tracked, the missing data was interpolated. This resulted in inaccurate shoreline locations and thus unsuccessful set boundary conditions. The dry sand is interpreted as wave breaking and as a result a dissipation peak is fitted over the dry sand (Figure 20a, b).

For all 962 planviews an imap was created. The imaps that were used as input for the model were hand selected, 334 imaps were rejected (35%) thus 628 imaps were used as input for the assimilation model. To reject images with e.g., raindrops, poor shoreline definition and sun glare (Figure 20c, d) was a time consuming process, however a necessary one. False images could have influenced the model, which is rather robust: 'a false image would nudge the updated bathymetry away from truth and would require a lot (order 10) of "good" images to nudge the bathymetry back' (Van Dongeren et al., 2008).

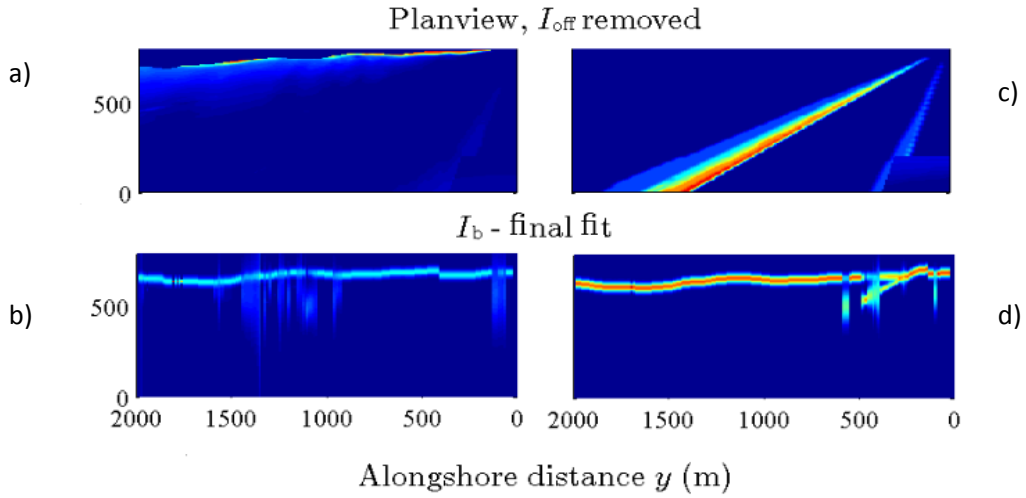

Figure 20 planview I_{off} removed with poor shoreline definition (a) resulting in a bad imap (b) on 04-07-2001 at GMT 19.00. Planview with sun glare (c) resulting in a bad imap (d) on 04-07-2001 at GMT 04.00.

Finally the roller energy dissipation rate (D_r) was derived from intensity maps (I), assuming that the high-intensity areas of wave breaking in the time-exposure video images are a proxy for D_r. Wave properties were measured with and approximate distance of 15km from the study site with a water depth of 18m. These wave properties were transformed to the image boundary, 7 m water depth, using the Battjes and Janssen (1978) wave transformation model. The intensity maps were scaled with the incoming wave energy flux to obtain a video-derived measure D_r.

$$D_r(x,y) = \frac{I(x,y)}{\int x \int y \, I \, dxdy} \int_y E c_g cos\theta dy \qquad (11)$$

where E (section2.1) the wave energy at the offshore boundary of the model, c_g is the wave celerity (Van Dongeren et al., 2008; Price & Ruessink, 2013).

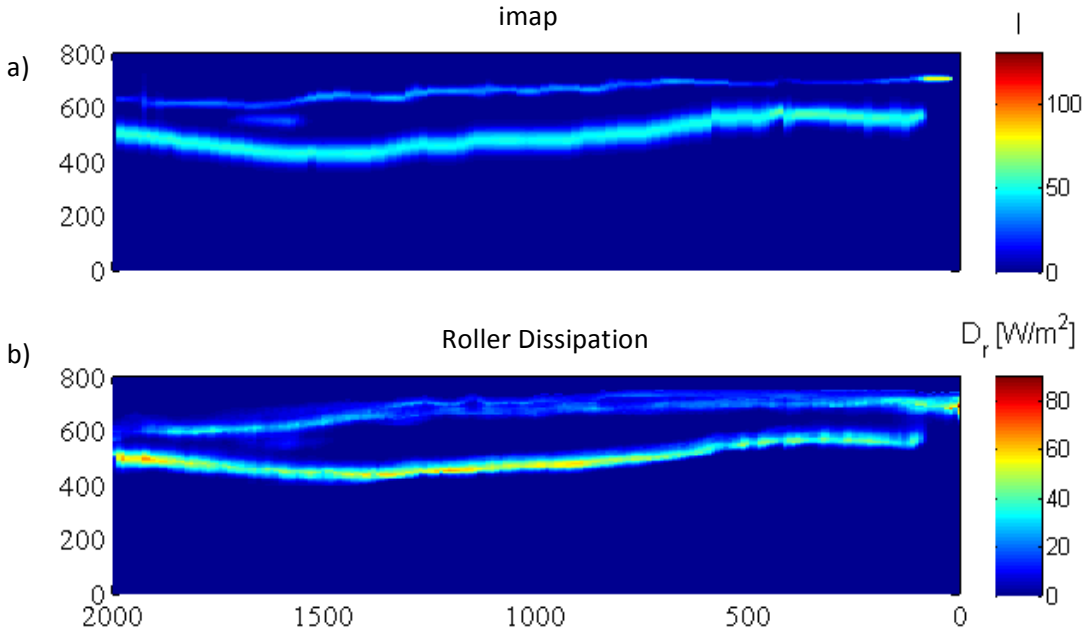

Figure 21 (a) Intensity map and (b) roller dissipation map on 09-08-2001 at GMT 14.00.

4.1.2. Improved initial bathymetric map

The initial bathymetric map that was described in section 3.2.3 did not show well developed sandbars. Therefore, the assimilation model was used to compute a more realistic initial bathymetric map. Roller dissipation maps between 9 July 2001 and 16 July 2001 were used to compute a bathymetric map where the sandbar was slightly developed, but where the SPAW had not emerged yet (Figure 22). The functioning of the assimilation model is described in section 4.2.

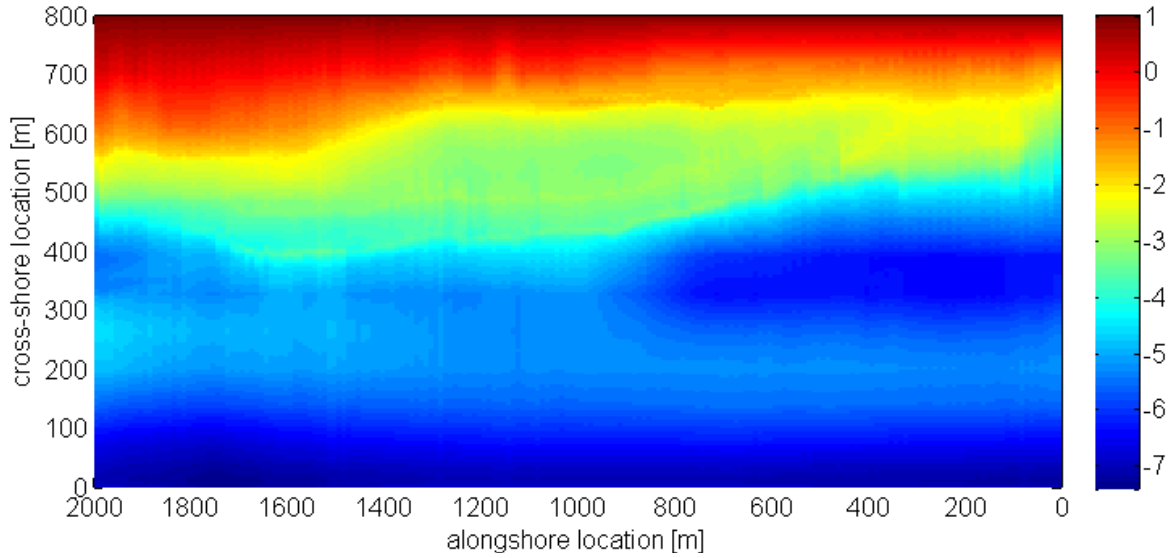

Figure 22 Bathymetric map at 16 July 2001. Where 800 on the x axis is onshore and 0 is offshore.

4.2. Assimilation process

The D_r maps (section 4.1) and the initial bathymetric map (section 3.2.3) were used to estimate the update of the bathymetry.

The model is based on a least squares estimator to update the bathymetry. It needs the prior state of the bathymetry h_{prior} as well as new estimates of bathymetry h_{obs}, the latter were obtained indirectly from D_r maps. The updated bathymetry is computed using:

$$h_{update} = h_{prior} + \alpha\,(h_{obs} - h_{prior}) \qquad (12)$$

where α is the optimal weighing factor and balances the uncertainties in between the prior and observed bathymetry. When the uncertainty of the observed D_r is large, α decreases and acts as a dampening factor. For low α, $h_{update} \approx h_{prior}$, hardly any weight is given to the new observed bathymetry. α can be computed as following:

$$\alpha = \frac{\sigma^2{}_{prior}}{\frac{T_S}{\Delta t}\sigma^2{}_{obs}\,\sigma^2{}_{prior}} \tag{13}$$

Van Dongeren et al. (2008) determined that the observations are not statistically independent, as such $\sigma^2{}_{obs}$ need to be multiplied by $\frac{T_s}{\Delta t}$, where T_s is the simulation duration for an images and Δt is the numerical time step. Subsequently the uncertainty for the updated bathymetry $\sigma^2{}_{update}$ can be computed:

$$\sigma^2{}_{update} = \alpha\ \frac{T_S}{\Delta t}\ \sigma^2{}_{obs} \tag{14}$$

For the next time step h_{update} and $\sigma^2{}_{update}$ will become h_{prior} and $\sigma^2{}_{prior}$. In Eq. (12) h_{obs} is mentioned, however no direct observations from the bathymetry were available for each time step. To solve this problem h_{obs} was derived from the roller dissipation maps.

$$h_{update} = h_{prior} - \ \alpha \left(\frac{\frac{dD_r}{d_h}}{\left(\frac{dD_r}{d_h}\right)^2 + \delta^2} \right)\ (D_r\ - D_{r_{obs}}) \tag{15}$$

where δ^2 is included in the formula as noise to avoid the denominator becoming zero (Van Dongeren et al., 2008).

h_{update} is computed for each cross-sectional profile during the study period, and thus forms the bathymetric maps (Figure 17).

The uncertainty in the observed data will be defined as the ratio between the sum of the measurement error and the difference between the modelled and observed quantity, and the square of the gradient with respect to depth.

$$\sigma^2{}_{obs} = \frac{\varepsilon^2 + (f - f_{obs})^2}{\left(\frac{df_i}{dh}\right)^2 + \delta_i{}^2} \tag{16}$$

Accordingly, when there is a large difference between I_b and D_r the uncertainty increases (Morris, 2013).

Due to the exclusion of imaps (discussed in section 4.1) there are periods where no input is available for the assimilation model. The uncertainty of the bathymetry increases during these periods. This increase in uncertainty is calculated using a sigmoid function:

$$\sigma^2(t_j) = \sigma^2(t_{j-1}) + (\sigma^2{}_{evo} - \sigma^2(t_{j-1}))\ tanh^2\left(\frac{3}{T_r}\left(t_j - t_{j-1}\right)\right) \quad (17)$$

where j is the index of the run, t_j is the Julian day, T_r is the rate at which the computed uncertainty is dominated by morphological change, and $\sigma^2{}_{evo}$ is the natural uncertainty of the bathymetry (0.6 m). The sigmoid functions such that the uncertainty in the bathymetry will gradually increase until T_r days where it will be equal to the natural uncertainty of the initial bathymetric profile (Van Dongeren et al., 2008; 2012; Morris, 2013).

The bias in D_r is computed in order to evaluate the results from the assimilation model. Positive bias in D_r is defined as I_b on average to be greater than D_r. The bias in D_r is calculated as an average absolute value and a total relative value for the entire domain.

$$Avarage\ Absolute\ Bias = \frac{1}{N}\sum_{i=1}^{N}\left(I_{b,i} - D_{r,com,i}\right) \quad (18)$$

$$Total\ Relative\ Bias = \frac{\frac{1}{N}\sum_{i=1}^{N} I_{b,i} - D_{r,com,i}}{\sum_{i=1}^{N} I_{b,i}} \quad (19)$$

Here, N is the number of grid points on a uniform grid, $I_{b,i}$ is the observed roller dissipation and $D_{r,com}$ is the computed roller dissipation. A positive bias in roller dissipation indicates that I_b is on average greater than D_r. Negative bias indicates the opposite from positive bias (Morris, 2013).

4.3. Quantitative analyses SPAW

The evolution of the bathymetric profile during the study period is displayed in 628 bathymetric maps. To be able to further analyze SPAW dynamics, SPAW width, length, height and volume were computed from every one in ten bathymetric maps, thus 62 maps. In this chapter the methods for extracting the SPAWs features from bathymetric maps are described.

The width and length were derived from the bathymetric images. In the bathymetric images the SPAW can easily be recognized by eye. First, the center of the SPAW was located by

manually selecting the highest point (red point in Figure 23 and Figure 24). This location was also used to determine the cross- and alongshore migration patterns of the SPAW. Secondly, the depth of the SPAW's adjacent trough was determined (white point in Figure 24). This depth was used as a base level. From the center of the SPAW, locations matching the trough depth plus 0.3 m were determined to be the edges of the SPAW. This value was determined by a careful examination of the cross-sections of several bathymetric maps. The threshold of 0.3 m with reference to the trough yielded the best outcome. This technique was used to locate L1 and L2, determining the length of the SPAW, and to find W1, the seaward point of the SPAW, determining the width (Figure 23). W2 was taken as the location at which the bed elevation of the landward part of the SPAW started to increase.

The height of the SPAW was both computed as a maximum and as an average with reference to the base level. The maximum height was derived from the bathymetric map using the coordinates from the center of the SPAW; subsequently the base level elevation was subtracted from this height. The average height was found by creating a polygon with L1, L2, W1 and W2; subsequently the average height within the polygon was computed.

The volume of the SPAW was calculated by making an approximation of the shape of the SPAW. The use of a polygon shape is motivated by the shape of the SPAW as observed in the time-exposure images during the study period; the shape of the white foam caused by the wave breaking over the SPAW resembles a polygon. Therefore the following equation was used to compute the SPAWs volume:

$$Volume = \pi * \left(1/2 * W\right) * \left(1/2 * L\right) * H \quad (17)$$

where W is width in m, L is length in m and H is the average height in m.

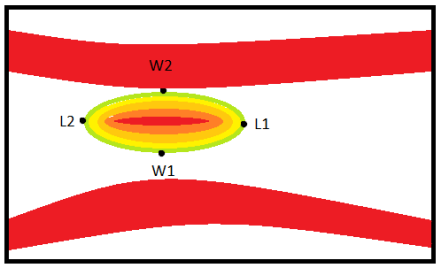

Figure 23 Schematic overview of locations determining the dimensions of the SPAW.

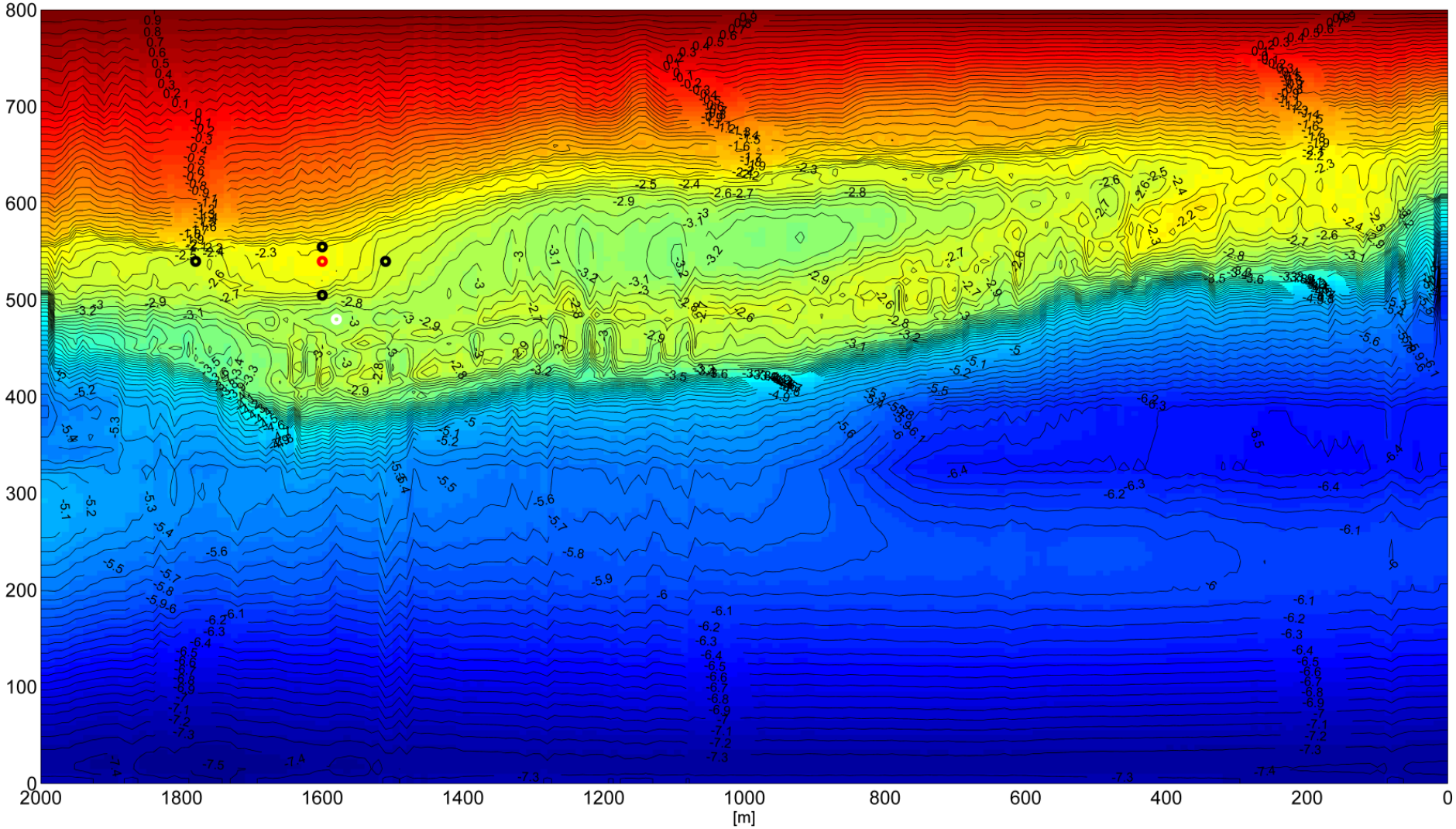

Figure 24 Bathymetric map with contour lines based on the elevation at 19-7-2001 GMT 0400. Red point is the Center of the SPAW. Black dots indicate the dimensions. White point is the trough location used as base level.

5. Bathymetric maps and extracted SPAW dimensions

Based on the 628 hourly bathymetric maps during the study period several analyses were performed, to better understand temporal and spatial variation of SPAW dynamics. First, bathymetric maps are described as a whole. Secondly, SPAW dimensions and the migration direction from the outer sandbar towards the inner sandbar are described. Finally, a connection between the dimensions, the dynamics and the wave conditions is formulated.

5.1. Bathymetric maps

Each bathymetric map comprises 200 cross-shore profiles with an alongshore spacing of 10m, resulting in an alongshore extent of 2 km. The cross-shore extent of the profile is 800 m with a 5 m resolution.

In general the bathymetric maps show four characteristic zones (Figure 25). Firstly, the intertidal beach can be observed between approximately x=700m-800m, with corresponding elevation values of 0m and higher. Secondly, the inner sandbar is located between approximately x=620m-700m. Thirdly, the outer sandbar is located between x = 400m-600m, the relatively large cross shore extent in which the outer bar can be observed is due its alongshore variability. Finally the SPAW is located between the inner and the outer bar, at alongshore distance y = 1400-1600m.

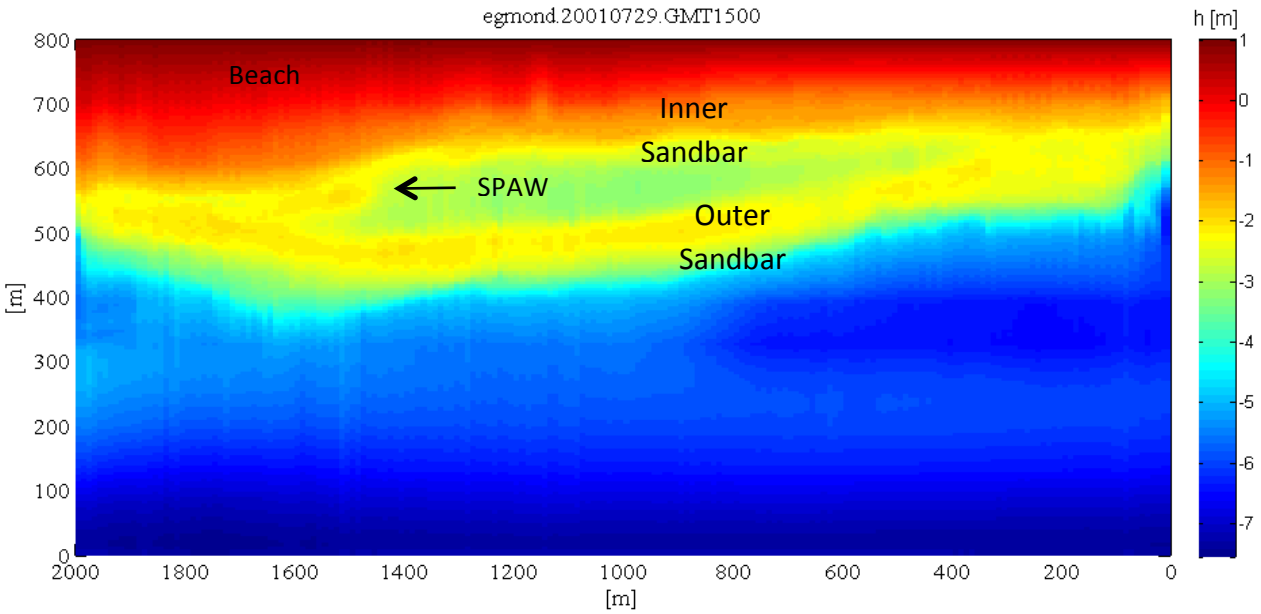

Figure 25 Bathymetric map on 29-07-2001 at GMT 15.00. On the map outer sandbar, SPAW, inner sandbar and beach are indicated. y=0 being offshore, y=800 being onshore

The first moment at which the SPAW could be observed in a bathymetric map, as having a peak that was not merged with a sandbar, was on 20 July 2001 GMT 0700. At this date however the SPAW was already closer to the inner sandbar than to the outer sandbar, indicating that the detachment of the SPAW was not captured in the bathymetric maps. Furthermore, the SPAW grew significantly during the evolution of the bathymetric maps however the SPAW did not show cross-shore migration.

The SPAW merged with the inner sandbar on 4 September 2001 GMT 11.00. As the centre of the SPAW remained at approximately the same cross-shore location this merge was not caused by cross-shore migration but by the SPAW growing towards the inner sandbar. In the bathymetric maps this can be seen as (i) the merge of contour lines of the SPAWs top with the contour lines of the inner sandbar's top (Figure 26a, b) and as (ii) the decrease in depth of trough between the SPAW and the inner bar to almost zero (Figure 26c, d).

Wijnberg and Holman (20017) defined SPAW duration as the moment from detachment until the moment of welding. Because the detachment of the SPAW was not captured, it would not be correct to define the period in which the SPAW was detectable in the bathymetric maps as SPAW duration. Therefore this period is named SPAW detection; the time the SPAW could be detected in the bathymetric maps was 46 days, from 20 July to 4 September.

The evolution of the bathymetric maps was not gradual, but incremental. These incremental changes appear to be linked to high wave events. More details about these incremental changes are given in section 5.3.

5.2. Dimensions

In this section the evolution of the SPAW dimensions that were extracted from the bathymetric maps are described, including length, width and height of the SPAW. As the SPAW detection period lasted from 20 July 2001 and 4 September 2001 the evolution of these dimensions is described for this period. Furthermore, the volume, which was computed from the dimensions, is described.

The evolutions of the dimensions show an increased during the study period (Table 3, Figure 27). The strongest increase is observed for the SPAW width (66%) during the detection

period. The least significant increase was observed for the average SPAW height (12%). The different evolution of the average and maximum height indicates that over time the slopes between the edges of the SPAW and the top of the SPAW have become steeper. The increase in maximum height was strongest between 6 August and 11 August. The percentage increase in volume was not taken into account, as this is a multiplication of the increase in width, length and height. The increased SPAW dimensions do not show a continuous, but an incremental increase (alternating grey and white boxes in Figure 27). The incremental changes can be divided in five periods. Three periods where the SPAW dimensions increase significantly, and two periods were there is nearly no evolution of the SPAW dimensions. In section 5.4 the (absent) changes are discussed in more detail.

Table 3 Information on the SPAW dimensions extracted from bathymetric maps during the detection period. *Units of volume are in m^3.

Dimension	Start (m)	End (m)	Change (m)	Average (m)	Growth Rate (m/day)	Steepest Increase	
						Period (2001)	*Rate (m/day)*
Width	50	83	33		0.7	05/08-12/08	1.4
Length	240	360	120		2.6	06/08-09/08	17
Height max	0.82	1.02	0.2		0.004	06/08-11/08	0.005
Height mean	0.63	0.71	0.09	0.7	0.001	-	-
Volume*	7500	15800	8300	11000	180	-	-

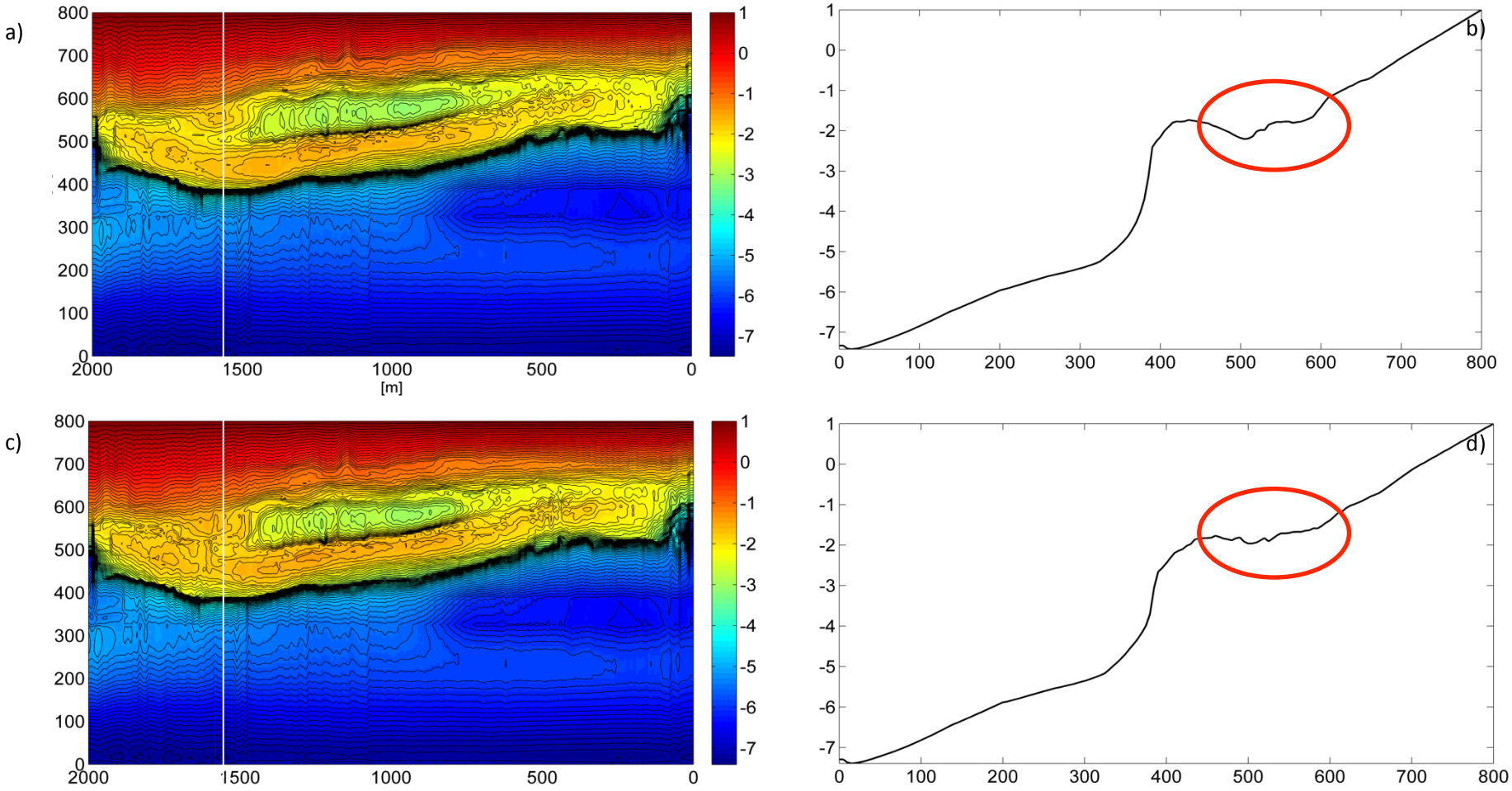

Figure 26 Bathymetric map at 04 September 2001 GMT 0700 before the SPAW has merged with the inner bar (a) and a bathymetric map at 04 September 2001 GMT 1100 just after the SPAW has merged with the inner bar (c). For both bathymetric profiles a cross-sections at the location of the SPAW is shown (y= 1600). The merge of the SPAW can be recognized by the absence of the trough in cross-section (d) compared to the trough in cross-section (b) indicated by the red oval.

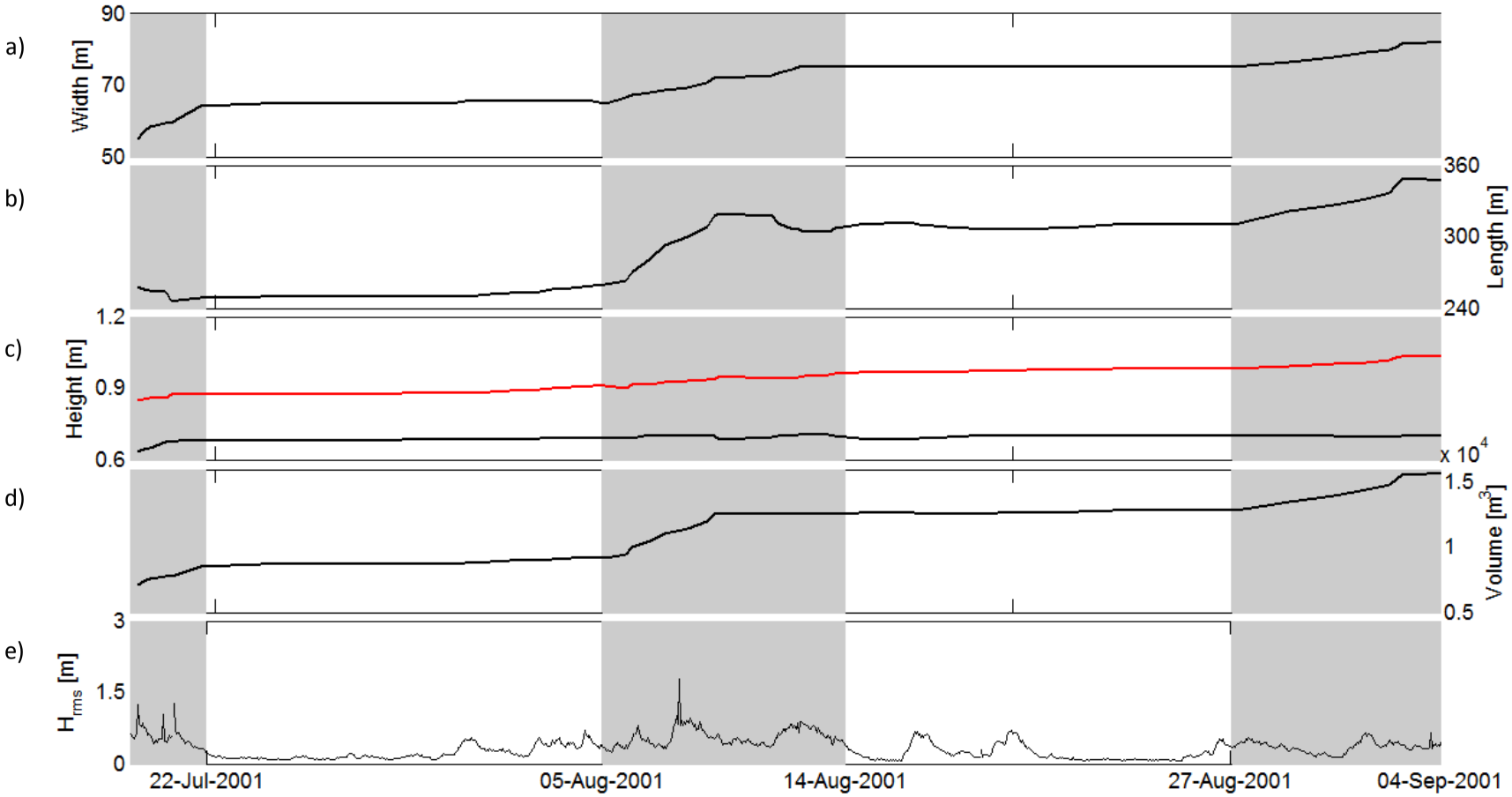

Figure 27 Width (a), length (b), height (c), volume (d) and wave power between 20-07-2001 and 04-09-2001. The grey areas indicate moment during which the wave power was high and subsequently caused the dimensions to respond and thus change.

5.3. Migration

The migration of the SPAW can be described both in terms of cross- and alongshore migration. In Section 5.1 was described that the cross-shore migration of the SPAW was not captured in the bathymetric maps based. The cross-shore migration according to the time-exposure images during the study-period is described in section 3.2.1. The alongshore migration, according to the highest point of the SPAW in the bathymetric maps, did show variations, described below.

From 20 July until 23 July the top of the SPAW moved towards the south, with a migration rate of 3 m/day. After the southward movement the SPAW remained at approximately the same alongshore location until 2 august, after which the top started to migrate north until 12 August (8 m/day). This northward migration was followed by a four day southward movement until 20 August (5 m/day). After 20 August the SPAW top remained on the same alongshore location until the SPAW attached to the inner sandbar on 4 September (Figure 28, Table 4). The conditions influencing the cross- and alongshore migration of the SPAW are discussed in section 5.4.

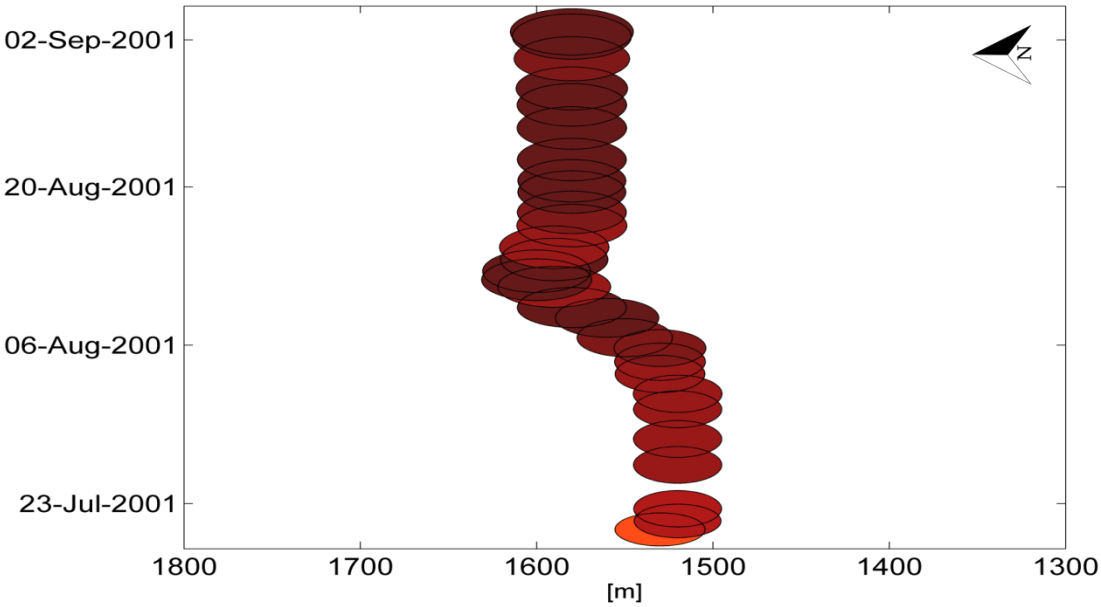

Figure 28 the x-axis indicates the alongshore position at which the centre of the SPAW was located at a specific time, indicated at the Yaxis. In the right corned the direction north is pointed out. The sizes of the red ovals indicate the actual size of the SPAW over time. The shade of red indicates the average height, with reference to the depth in the nearest trough +0.3 m, of the SPAW, darker red being higher.

Table 4 Three periods during the detection period where the SPAW migrated alongshore.

Period		Direction	Distance (m)	Rate (m/day)
20 July	**- 23 July**	South	10	3
2 August	**- 12 August**	North	80	8
12 August	**- 16 August**	South	20	5

5.3. Conditions influencing the SPAW lifecycle

In this section an attempt is made to point out the natural conditions that influence SPAW generation, migration and decay. To be able to make analyses of the whole life cycle of the SPAW the results from the assimilation model were complemented with information derived from planview images during the study period. The SPAW event according to the time-exposure images was described in section 3.2.2.

5.3.1. Formation

As the assimilation model did not capture the generation of the SPAW, the conditions influencing the formation are described according to time-exposure images. Before the detachment of the horn, waves were low to intermediate; this allowed the outer sandbar to develop a profile with strong crescentic patterns, as described in section 2.2. High waves after this calm period caused the offshore migration of the sandbar, driven by undertow (section 2.2). Part of the sandbar (the horn), however, remained on its original location, and a couple days later detached completely from the outer sandbar.

5.3.2. Migration and evolution

In this section the period between the detachment and the decay is discussed. This includes the cross-shore migration, alongshore migration and the dimensions of the SPAW. As the cross-shore migration was not captured in the bathymetric maps that topic is discussed according to time-exposure images from the study period.

Cross-shore migration

The SPAW migrated from the outer bar to the trough relatively quick (within seven days); the SPAW then remained in the trough for approximately 45 days. The waves were relatively high when the SPAW moved out of the trough towards the inner sandbar (3 August to 4 August). Indicating that the energetic conditions associated with high waves moved the SPAW out of the trough. In section 2.1 was described that waves migrate in deep water with a perfect symmetric sinusoidal shape. As waves enter more shallow water they start to feel

the bed and deform, in the sense of skewness and asymmetry. High waves become more skewed and asymmetric over a shallow bed, compared to low waves over the same shallow bed; this might have led to an increased onshore-directed sediment transport pushing the SPAW out of the trough.

Alongshore migration

The direction of the alongshore migration op the SPAW top was discussed in section 5.2. In the detection period there were three periods during which the SPAW showed variations in the evolution of the alongshore migration. These three periods correspond to high wave events, and also to period that show large variations for P_y. However, for this study, no relation was found between the direction of P_y and the migration direction of the SPAW top.

The absence of this relation indicates that the model functioning might have influenced the alongshore migration of the SPAW top, this topic is further discussed in section 6.1.

Evolution dimensions

The evolution of the SPAW dimensions is not continuous but incremental. The detection period van be divided in five periods; three of which show significant growth of the SPAW dimensions, and two periods were the evolution of the dimensions is almost absent. These three periods correspond to periods with high waves (grey boxes in Figure 27). High waves, can become increasingly non-linear causing sediment transport to increase, and thus explain the different evolution patterns during high and during low waves. However, considering the unnatural, incremental pattern, other factors, such as the models functions might have influenced the SPAW evolutions. The influence of the model functions on SPAW evolution is further discussed in section 6.1.

5.3.3. Welding with inner bar

Before the SPAW welded with the inner bar, it was separated from the sandbar by a trough. This trough was filled with sediment in approximately five hours, causing the SPAW to be welded with the inner sandbar. This sediment appeared to have been eroded from the SPAW top, whose height decreased with 25% in those five hours. The welding of the SPAW with the inner sandbar took place during a period with high waves, indicating that wave non-linearity was the driving mechanism of this process.

6. Discussion

This chapter aims to discuss both the functioning of the assimilation model and the results from the analyses. Firstly, the discussion concerning the model will include both the process towards creating the input for the model as the models functioning. Secondly, the results from the analyses are compared to previous SPAW research.

6.1. Model functioning

The assimilation model has shown that it is able to integrate a SPAW in bathymetric maps. Unfortunately, no high-resolution field measurements were available to compare the results with. It is therefore even more important to evaluate the models functioning extensively. The results are dependent on several choices that were made concerning e.g. parameter values, threshold values and bathymetric input. Both models functioning and the choices that were made deserve further discussion.

As the Imaps were directly derived from planviews they correspond directly to observed dominant features. This does not apply for the bathymetric maps; bathymetric updates show a short delay compared to the imaps. When imaps were absent, or did not show a SPAW the bathymetric map did not update the SPAW profile. As soon as the imap showed a SPAW it took the bathymetric map on average four simulation runs to update the SPAWs profile (Table 5). The delay is inherent to the assimilation process in which a Kalman-type filter (α) is applied. Nevertheless, dominant features in the imaps are translated to the bathymetric maps by the assimilation model, making the delay acceptable.

Table 5 overview of examined cases where the evolution of the SPAW showed a delay compared to the evolution of the imap.

Case	Appearance SPAW Imap	Update SPAW Bathymetry map	Delay (hours)
1	19-07-2001 GMT 16.00	20-07-2001 GMT 06.00	5
2	31-07-2001 GMT 15.00	31-07-2001 GMT 19.00	4
3	03-08-2001 GMT 06.00	03-08-2001 GMT 09.00	3
4	04-08-2001 GMT 08.00	04-08-2001 GMT 11.00	3

In section 5.4.2 the incremental evolution of the bathymetric maps were described. As these changes do not appear to be natural other factors might have influenced the evolution of the dimensions, and thus the updates of the bathymetric maps.

In section 5.4 was mentioned that the model functions might have influenced the incremental evolution pattern of the SPAW. Two factors with the functioning of this model were found that contributed to these incremental changes.

The first factor is related to the difference between I_b and D_r, which can be expressed in terms of total relative bias. Decrease in bias indicates that the difference between the observed and computed roller dissipation decreases, vice-versa increase in bias indicates that the difference between the observed and computed roller dissipation increases. A negative relation was found between the total relative bias in roller dissipation and wave height: the bias decreases with increasing wave height (Figure 29). The relations described in Eq. (13) and Eq. (17) show that an increased total relative bias results in a low α, dampening the effect of an update on the prior bathymetry, while a decrease total relative bias results in a high α, not the effect of an update on the prior bathymetry.

The relation, within the mode, between wave height and bathymetric updates, might have enhanced the natural effect of high waves and low waves on sediment transport.

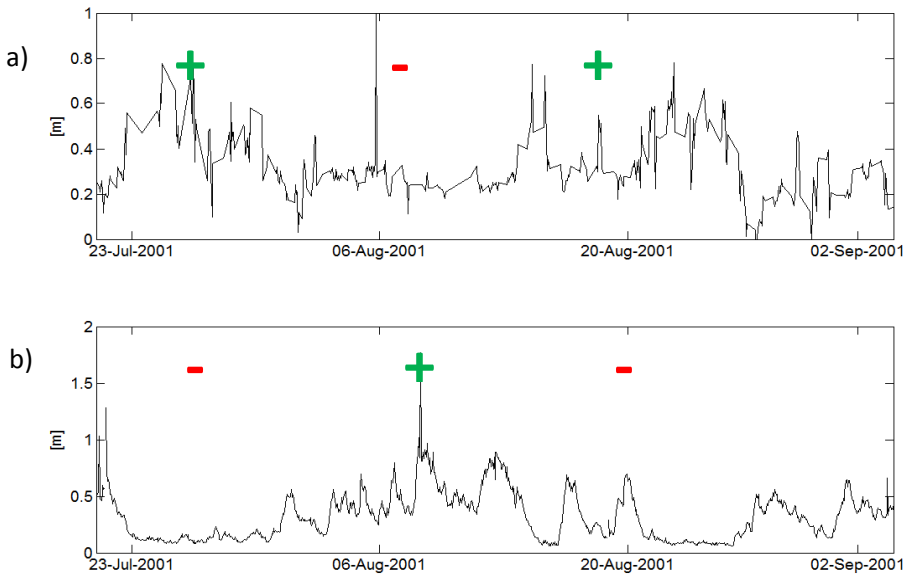

Figure 29 Total relative bias (a) and wave height (b) between 20-07-2001 and 04-09-2001. Green + and red – periods with relatively high and relatively low values, respectively.

A possible explanation for bias between D_r and I_b is that the constant wave breaking parameter (ϒ) might not be appropriate. When using a wave breaker parameter, that is too large, waves break closer to the shore; this might indicate why not all energy is distributed over the dissipation peaks (Morris, 2013; Van Dongeren *et al.*, 2008). A wave breaking parameter dependent on wave conditions could decrease the positive bias, and thus the uncertainty of the bathymetry (Van Dongeren *et al.*, 2008; Price and Ruessink, 2013; Morris, 2013).

The second factor that could have influenced the incremental SPAW evolution is related to the certainty of the bathymetry. During low wave periods the Gauss-Newton method was not always able to successfully fit Gaussian curves, resulting in the exclusion of imaps. The relation described in Eq. (17) shows that the uncertainty in the bathymetry with absent input will gradually increase until T_r days where it will be equal to the natural uncertainty of the initial bathymetric map (Morris, 2013; Van Dongeren et al, 2008). Thus, a relation exists between wave height and the evolution of the $\sigma^2(t_j)$ (Figure 30) Subsequently, the $\sigma^2(t_j)$is used to make the translation from σ^2_{obs} to σ^2_{prior}, where σ^2_{prior} is used in Eq. (13) to compute the α. As such high a σ^2_{prior} value decreases the α, and could dampen the update of the next bathymetric map, possibly contributing to the little variation shown in these periods.

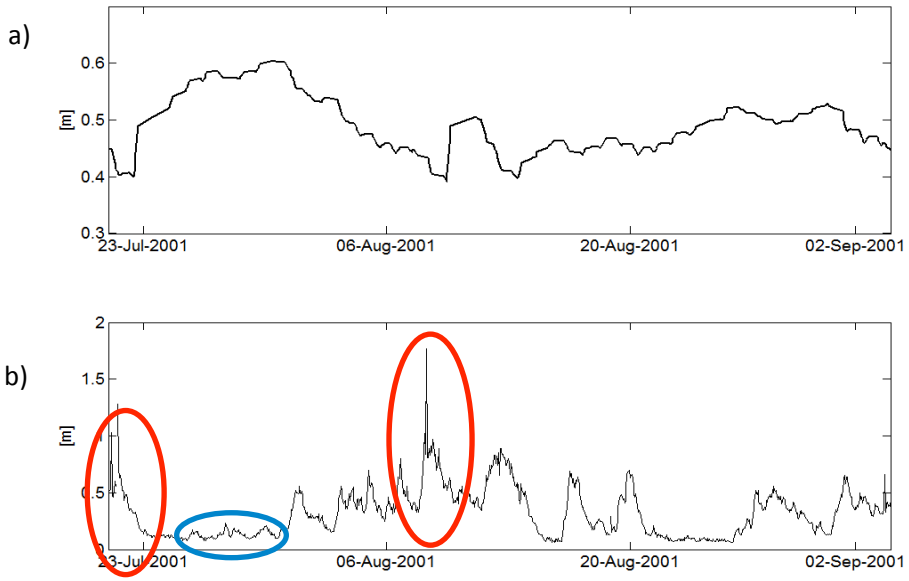

Figure 30 $\boldsymbol{\sigma^2(t_j)}$over the entire domain (a) and the H_{rms} from 20-07-2001 till 04-09-2001. Red ovals indicate high wave conditions and the blue oval indicates low wave conditions.

6.2. Comparing Results

The results from the assimilation model were carefully described and analyzed in chapter 6. In this section the results are compared to results from other studies addressing SPAWs.

Formation

The generation of the SPAW during the study period was caused by the offshore migration of the outer sandbar, while the horn of the bar remained at the same location. This is the same mechanism as described by Shand (2010), which he referred to as bar splitting, and Almar et al. (2010). Wijnberg and Holman (2007) and Van der Weerd (2012) did not describe the offshore migration of the outer sandbar during the SPAW generation.

Migration

Dimensions –The SPAW width and length extracted from the time-exposure images during the study period were 52 m and 226 m, respectively (Van Kuik, 2016). With the results from the assimilation model the average SPAW width and length during the study period were found to be 70 m and 300 m, respectively. In the literature study the average volume of all SPAWs was computed with an average height of 0.5 m (from Duck). The volume of the SPAW event according to the width and length of the time-exposure images and the height extracted from the bathymetric maps (0.7 m) is 6000m3, which is low compared to the average volume extracted from the bathymetric maps, 11000m3. The discrepancy between these values can be caused by two factors; the dimensions that extracted from the bathymetric maps are strongly depended on the chosen threshold for determining the location of L1, L2 and W1, in addition; the method to determine SPAW width and length from time-exposure images is also flawed. As such, comparing observed and computed values for dimensions is proving difficult.

In section 2.3.5 was hypothesised that the relatively large SPAW volume for LTV was linked to sandbar wavelength and amplitude. The SPAW volume in Egmond aan Zee computed with the information from the assimilation model is significantly higher than the volume for Duck; confirming the hypothesis that states that sandbar wavelength and amplitude are related to SPAW volume.

Cross-shore migration - In this modelling study, the time between the first detection of the SPAW and the welding with the inner sandbar was 46 days. The average transit time for a

SPAW in Egmond is 38 days (Van Kuik, 2016). However this is a hard comparison to make, as not the whole lifecycle of the SPAW was captured by the modelling study.

Previous observational studies and a modelling study showed that the SPAW transited the trough either between the outer and the inner sandbar or the inner sandbar and the SPAW as an intact form. The evolution of the SPAW in the bathymetric maps, however, shows was growing during the detection time. A possible explanation is that the bathymetry is still updated according to the initial bathymetric maps.

Alongshore migration - The alongshore migration of the SPAW was measured such that the highest location of the SPAW determined its position. As the variations in the alongshore positions of the SPAW top coincide with variation in the SPAW dimensions it can be stated that location of the SPAW top in strongly influenced by the evolution of the SPAW dimensions. In retrospect it would have been better if a volume study was performed in order to determine the locations of the SPAWs centre. This might have resulted in a more realistic migration pattern. However, according to the time-exposure images, the SPAW did migrate alongshore. Previous studies on SPAW dynamics state that SPAWs migrate onshore remaining on its alongshore position. Evaluation of more SPAW events at Egmond aan Zee might be able relate local wave conditions to the direction of the alongshore migration.

Decay

Van der Weerd (2012) stated that the onshore migration of the SPAW is driven by erosion on the seaward side of the SPAW and accretion of the landward side of the SPAW. The results from the assimilation model have shown that just before the SPAW welded with the inner sandbar, the top of the SPAW eroded; subsequently the eroded material was deposited in the trough between the SPAW and the inner bar. This mechanism might add to the mechanisms described by Van der Weerd (2012).

7. Conclusion and recommendations

7.1. Conclusion

SPAW features were objectively derived from time-exposure images by locating an intensity peak between cross-shore location of the inner and the outer sandbar that exceeded the threshold 1. This threshold was found by trial and error, and proved the best results. Furthermore, peaks between the inner and the outer bar might have been misidentified, therefore only when peaks in between the inner and the outer bar in five or more subsequent cross-sections exceeded the threshold the peaks was defined a SPAW.

The bathymetric maps during the study period clearly showed the presence of the SPAW. To extract the SPAW dimensions from the bathymetric maps the edges of the SPAW were localized according to the depth of a variable reference point in the nearest trough. The depth in the reference point plus 0.3 m defined the edges of the SPAW. To compute the volume of the SPAW the assumption was made that the SPAW was shaped as an oval.

The bathymetric maps did not capture the detachment of the SPAW, and the feature also remained at approximately the same cross-shore location.

According to the time-exposure images and wave data could be established that during a relatively high wave event the SPAW was generated by the offshore migration of the outer sandbar, while the horn of the sandbar remained at its original location, becoming the SPAW.

The analyses of the bathymetric maps and the evolution of the SPAW dimensions showed that the SPAW grew during its onshore migration. The length, width, maximum height and volume grew 120 m, 33m, 0.2 m and 8300 m^3. The evolution of this growth was not continuous but incremental, these incremental changes are linked to two factors; firstly, the relation between wave height and sediment transport, secondly the relation between wave height and the certainty in the bathymetry influencing the models functions.

7.2. Recommendations

For future research I suggest that the computation of the imaps with the Gauss-Newton method is improved, such that the number of imaps that are excluded from the study decrease. A denser input for the assimilation model might result in a less incremental evolution of the bathymetry. Another model input that could be improved is the initial bathymetric map. The resolution of the bathymetric map extracted from JarKus is of such low resolution that after the interpolation no nuance is left in the map. An initial map that resembles the true bathymetry more closely, might lead to a bathymetry evolution that also is more realistic.

The methods that I used to determine the SPAW dimensions are not fully automated, and not fully objective. Possibilities within remote sensing and pattern recognition should be further investigated.

Finally, combining time-exposure images and wave data in an observational study can still provide many new insights in SPAW dynamics, which might help the improvement of models like Beach Wizard.

8. Literature

Aagaard, T., Davidson-Arnott, R., Greenwood, B., Nielsen, J. (2004). Sediment supply from the shoreface to dunes: linking sediment transport measurements and long-term morphological evolution. *Geomorphology, 60*: 205–224.

Almar, R., Castelle, B., Ruessink, B.G., Senechar, N., Bonneton, P., Marieu, V. (2010) Two- and three- dimonesional double-sandbar system behavior under intense wave forcing and meso-macro tidal range. *Continental Shelf Research, 30:* 781-792.

Battjes, J.A., Sobey, R.J., Stive, M.J.F. (1990) Nearshore circulation. In Mehaute, B. Hanes. D.M. (pp. 1192-1210, Global Coastal Ocean- multiscale interdisciplinary processes. Harvard University press, Cambridge, Massachusetts and London.

Bolle, A., Wang, Z.B., Amos, C., De Ronde, J. (2010) The influence of changtes in tidal asymmetry on residual sediment trnasport in the Western Scheldt. *Cont. Shelf. Res.* 30, 871-882.

Bowen, A. J., and D. L. Inman (1969) Rip currents, 2, Laboratory and field observations. *Journal of Geophysical Research*. 23: 5479-5490.

Bryan, K. R., and A. J. Bowen (1997) Can bar-trapped edge waves cause bar formation, bar movement or bar growth? *in Pacific Coasts and Ports '97 Conference*, pp. 1037–1042, Cent. for Adv. Eng., Univ. of Canterbury, Christchurch.

Castelle, B., and Ruessink, B.G. (2011) Modelling formations and subsequent nonlinear evolution of rip channels: Time varying versus time-invariant wave forcing. *Journal of geophysixal research. 116:* 2156-2202.

Castelle, B., Ruessink, B.G., Bonneton, P., Marieu, V., Bruneau, N., Price, T.D. (2010) Coupling mechanisms in double sandbar systems. Part 1: Patterns and physical explanation. *Earth Surf. Process. 35:* 476-486. (a)

Castelle, B., Ruessink, B.G., Bonneton, P., Marieu, V., Bruneau, N., Price, T.D. (2010) Coupling mechanisms in double sandbar systems. Part 2: Impact on alongshore variability of inner bar rip channels. *Earth Surf. Process., 35:* 771-781. (b)

Coco, G., Murray, B.G. (2007) Patterns in the sand: From forcing templates to self-organization. *Geomorphology, 91:* 271-290.

De Ronde, J.G. (2008). Toekomstige langjarige suppletiebehoefte. Deltares report Z4582.24, september 2008.

Enckevort, I.M.J., Ruessink, B.G., Coco, G., Suzuki., K., Turner, I.L., Plant, N.G., Holman, R.A. (2004) Observations of nearshore crescentic sandbars. *Journal of geophysical research, 109,* C06028, doi:10.1029/2003JC002214.

Enckevort, van, I.M.J., Ruessink, B.G. (2002) Video observations of nearshore bar behavior. Part 1: alongshore uniform variability. *Continental Shelf Research, 23:* 501-512. (a)

Enckevort, van, I.M.J., Ruessink, B.G. (2002) Video observations of nearshore bar behavior. Part 2: alongshore non-uniform variability. *Continental Shelf Research, 23:* 501-512. (b)

Greenwood, B., & Davidson-Arnott, R. G. (1975). Marine bars and nearshore sedimentary processes, Kouchibouguac Bay, New Brunswick, Canada. *Nearshore sediment dynamics and sedimentation*, *16*, 123-150.

Holman, R.A., Haller, M.C. (2013) Remote Sensing of the Nearshore. *Annu. Rev. Mar. Sci., 5:* 95-113.

Holman, R.A., Stanley, J. (2007) History and technical capabilities of Argus. *Coastal Engineering, 54:* 477-491.

Konicky, K.M., Holman, R.A. (2000) The statistics and kinematics of transverse sand bars on an open coast. *Marine Geology, 169:* 69-101.

Koster, L. (2006) Humplike nourishing of the shore face, Deltares, Delft.

Lageweg, van de, W.I., Bryan, K.R., Coco, G. & Ruessink, B.G., 2013. Observations of shoreline-sandbar coupling on an embayed beach. *Marine Geology*, 344, 101-114.

Lane, A.C. (1888) The geology of Nahant. *Boston Soc. Natur. Hist*. 91-95.

Longuet-Higgins, M.S. and R.W. Stewart (1964). Radiation stresses in water waves; a physical discussion, with applications. *Deep Sea Research and Oceanographic Abstract*. 11, 529-562.

Masselink, G., and Hughes, M.G. (2003). Introduction to coastal processes and geomorphology. London, UK, Hodder Arnold.

Morris, J. (2013) *Estimation of the Nearshore Bathymetry using Remote Sensing Techniques*. (Master Thesis, Deltares). Retrieved from: repository.tudelft.nl/assets/uuid:c2b51c70-7ff2-46c8-bc0c.../Final_Verision.pdf.

Price, T.D., Castelle, B., Ranasinghe, R., Ruessink, B.G. (2013) Coupled sandbar patterns and obliquely incident waves. *J. Geophys. Res., Earth Surf., 118:* 1677-1692.

Price, T.D., Ruessink, B.G. (2012) Observations and conceptual modelling of morphological coupling in a double sandbar system. *Earth Surf. Process. Landform, 38:* 447-489.

Price, T.D., Ruessink, B.G., Castelle, B. (2014) Morphological coupling in multiple sandbar systems – a review. *Earth Surf. Dynam., 2:* 309-321.

Price, T.D., Ruessink. B.G. (2011) State dynamics of a double sandbar system. *Continental Shelf Research, 31:* 659-674.

Ruessink, B.G., Coco, G., Ranasinghe, R., Turner, I.L. (2007) Coupled and noncoupled behavior of three dimensional morphological patterns in a double sandbar system. *J. Geophys. Res., 112,* C07002, doi:10.1029/2006JC003799.

Shand, R.D. (2007) Bar splitting: system attributes and sediment budget implications for a net offshore migrating bar system. *Journal of Coastal Research,* SI 50 (Proceedings of the 9th International Coastal Symposium), pg-pg. Gold Coast, Australia, ISBN.

Short, A.D., Agaard, T. (1993) Single and multiplw-bar change models. *Journal of Coastal Research.* 15, 141-157.

Sonu, C.J. (1973) Three-dimensional beach changes*. Journal of Geology.* 81, 42–64.

Thiebot,J., Idier, D., Garnier, R., Falques, A., Ruessink, B.G. (2012) The influence of wave direction on the morphological response of a double sandbar system. *Continental Shelf Research, 32:* 71-85.

Van der Weerd, L. (2012) Wave-driven dynamics of shoreward propagating accretionary waves in the nearshore, Deltares, Delft.

Van Dongeren, A., Plant, N.G., Cohen, A., Roelvink, D., Haller, M.C., Catalan, P. (2008) Beach Wizard: Nearshore bathymetry estimation trhough assimilation of model compuations and remote observations. *Coastal Engineering, 55:* 1017-1027.

Van Dongeren, A., Van Ormondt, M., Sembiring, L., Sasso, R., Austin, M., Briere,C., Swinkels, C., Roelvink, J.A., Van Thiel De Vries, J.S.M. (2013) Rip current predictions through model-data assimilation on two distinct beaches. Paper presented at: *Coastal Dynamics 2013: 7th International Conference on Coastal Dynamics, Arcachon, France, 24-28 June 2013*. Retrieved from:http://repository.tudelft.nl/islandora/object/uuid:8dee0408-1e71-4899-b37251bfd8a52895/?collection=research.

Van Kuik, N. (2016) *The effect of shoreface nourishments on Shoreward propagating Accretionary Wave* (Bachelor Thesis, University Utrecht)

Van Rijn, L.C. (2007). Unified View of Sediment Transport by Currents and Waves. I: Initiation of Motion, Bed Roughness, and Bed-Load Transport. Journal of Hydraulic Engineering, 133. 649 – 667.

Van Rijn, L.C. (2007a). Unified View of Sediment Transport by Currents and Waves. II: Suspended Transport. Journal of Hydraulic Engineering, 133. 668 – 689.

Wijnberg, K.M., Holman. R.A. (2007) Video-observations of shoreward propagating accretionary waves. *Proceedings of RCEM2007,* 737-743.

Wright, L.D., Short, A.D. (1984) Morphodynamic variability of surfzones and beaches: a synthesis. *Mar. Geol., 56:* 93-118.

Acknowledgements

For one year I have been working on this research, it was a year where I learned that doing your own research comes with really big ups, but also with downs. First I would like to thank my two supervisors, Timothy Price and Gerben Ruessink, for giving me the freedom to explore the possibilities of the model, and taking the time to brainstorm for solutions to solve problem that I encountered. Furthermore, I would like to thank my partner in crime Sara, we worked alongside each other for a year, and I consider the GIS room on the 8th floor a little bit as our home. Jan, for always being there when I came home happy about positive results, or when I came home feeling like everything was going wrong. Many friends read pieces of text, thank you all for helping me. And finally, I want to thank my parents, who always support me in everything I want to pursue.